This report was submitted as partial fulfillment of the requirements for a Master's Degree in Aeronautical Engineering at the University of Michigan in May, 1950.

AN INVESTIGATION OF THE EFFECTS OF A SIDE CONTROL JET ON THE NORMAL FORCE, DRAG, AND MOMENT OF AN AIRBORNE BODY IN SUPERSONIC FLIGHT

BY

LCDR C.A. Pierce, Jr. USN

LT. C.E. Craven, USN

TABLE OF CONTENTS

	Page
List of Figures and Tables	iii
List of Symbols Used	v
Summary	1
Introduction	2
Equipment and Procedure	4
Results and Discussion	13
Conclusions	23
Recommendations	24
Sample Calculations	25
Appendix A.	30
Appendix B.	37
Appendix C.	38
References	39

LIST OF FIGURES AND TABLES

Figure No.		Page
1	Picture of Model	40
2	Reproduction of a Portion of the Model Blueprint Showing Dimensions of the Model.	41
3	Schematic Diagram of the Test Set-up	42
4 - 12	P_h/P_1 vs P_o/P_1 For Each Pressure Tap For Each of the Three Configurations Tested.	43-51
13	Plot of $\Delta P_h/P_1$ Over the Body.	52
14	Integration of Station C of Figure 13.	53
15	Approximate High Pressure and Low Pressure Zones Due to Jet $\alpha = 0^\circ$, Straight Nozzle.	54
15a	General Shock Configuration and General Flow Pattern Due to the Jet.	55
16	Approximate High Pressure and Low Pressure Zones Due to Jet $\alpha = 14^\circ$, Straight Nozzle.	56
17	Approximate High Pressure and Low Pressure Zones Due to Jet $\alpha = 14^\circ$, Divergent Nozzle.	57
18	Schlieren Showing Jet Return to Tail $\alpha = 0^\circ$, Straight Nozzle.	58
19	Schlieren Showing Jet Return to Tail $\alpha = 14^\circ$ Straight Nozzle.	59
20	Shock Effects Produced by Straight Nozzle $\alpha = 14^\circ$.	60
21	Shock Effects Produced by Divergent Nozzle (Lower Mass Flux) $\alpha = 14^\circ$.	61
22	Schlieren Illustrating Shock Formed Outside the Jet $\alpha = 0^\circ$, Straight Nozzle.	62

LIST OF FIGURES AND TABLES (Cont'd)

Figure No.		Page
23	Schlieren Illustrating Shock Formed Outside the Jet α = 14°, Straight Nozzle.	63
24	Shadowgraph α = 14°, Straight Nozzle.	64
24a	Schlieren Showing Meniscus Formation in Jet; Tunnel Inoperative, α = 14°, Straight Nozzle.	65
25	Heavy Boundary Layer Build-up at α = 14°, No Jet.	66
26	P_h/P_1 vs x . α = 14°, No Jet.	67
27	ΔC_N, ΔC_D, $\Delta C_{M_{CG}}$ Obtained From Integration α = 0° Straight Nozzle.	68
28	ΔC_N, ΔC_D, $\Delta C_{M_{CG}}$ Obtained From Integration α = 14°, Straight Nozzle.	69
29	ΔC_N, ΔC_D, $\Delta C_{M_{CG}}$ Obtained from Integration α = 14°, Divergent Nozzle.	70
29a	Representative Manometer Board Photograph.	71
30	Shock Meniscus Length vs P_o/P_1.	72
31	Shock Meniscus Length vs. m_j .	73

Table No.		Page
1	P_h/P_1 At Each Orifice	74 and 75
2	Results of Integration of Pressure Distribution	76
3	Meniscus Length l in cm. vs. P_o/P_1	77
4	Variation of Meniscus Length (l) With P_o/P_1 and with m_j	78

LIST OF SYMBOLS USED

U_1 Tunnel free stream velocity (ft./sec.)

P_1 Tunnel static pressure (lbs./ft.^{2})

ρ_1 Tunnel air density (slugs/ft.^{3})

μ_1 Tunnel absolute viscosity (slugs/ft.sec.)

T_1 Tunnel static temperature (^{0}R)

D Model maximum diameter (ft.)

d Jet diameter at the throat (ft.)

P_o Jet stagnation pressure (lbs./ft.^{2})

ρ_j Jet air density (slugs/ft.^{3})

μ_j Jet absolute viscosity (slugs/ft.sec.)

U_j Jet velocity at the throat (ft./sec.)

T_o Jet stagnation temperature (^{0}R)

P_h Static pressure on the body (lbs./ft.^{2})

a_j Local speed of sound at the jet throat

R Gas constant, 1715 ft.^{2}/sec.^{2} ^{0}F

γ Ratio of specific heats of air, 1.400

θ Angle around body measured from top of body in degrees

m_j Mass flux from the jet (slugs/sec.)

$C_{M_{CG}}$ Moment coefficient about the center of gravity where the center of gravity is assumed to be on the side-jet centerline

C_N Normal force coefficient

C_D Drag coefficient

α Angle of attack (degrees)

SUMMARY

An experimental investigation was conducted to determine the effect of a side control jet upon the normal force, drag, and moment about the center of gravity of a cone-cylinder type of body in a supersonic stream. The jet issued perpendicular to the longitudinal axis of the body and was assumed to be located at the center-of-gravity of the body. The effect of this jet was investigated as a function of pressure ratio (jet stagnation pressure to tunnel static pressure), angle of attack, and jet throat diameter. Investigations were made at a constant tunnel Mach number of 1.90. Various pressure ratios of the jet (P_o/P_1) were used, but only two angles of attack and two jet throat diameters were used for the investigation.

Normal force and drag increased as a result of the side jet action on the pressure distribution around the body, and a moment was created about the center-of-gravity of the body.

This investigation was conducted at the University of Michigan Supersonic Wind Tunnel in April 1950.

INTRODUCTION

If a supersonic jet were to issue perpendicularly into a supersonic stream flowing past the jet, an aerodynamic disturbance would be created in the supersonic stream. In order to investigate the magnitude of this disturbance, two possible experimental methods were considered. The first consisted of allowing a supersonic jet, having its exit flush with the tunnel wall of the test section, to issue perpendicularly to the stream of a supersonic wind tunnel. The second consisted of placing a body in the test section of a supersonic wind tunnel and allowing a supersonic jet, having its exit flush with the body surface, to issue perpendicularly to the stream. The first method was discarded in order to avoid the boundary layer build-up along the tunnel wall (Ref. 1.). The second method was chosen for two reasons. First, the boundary layer build-up along the body would be small, as compared to the first method. Second, it permitted a three dimensional similarity to a body in actual flight that would make use of a side control jet.

Having chosen the second method, an investigation was undertaken in a supersonic wind tunnel. This investigation was made to determine the trend of the aerodynamic effect of a side control jet on the normal force, drag, and moment

about the center of gravity of a supersonic body (center of gravity assumed on the centerline of the side jet). In order to keep this investigation similar to conditions in flight, where aerodynamic effects would be felt, it was decided to simulate as closely as possible the conditions experienced from sixty to one hundred thousand feet: It was assumed that below sixty thousand feet ordinary control surface would be sufficient for any required maneuvering; therefore, the side control jet would not be needed. Above one hundred thousand feet aerodynamic effects are so small as to be negligible and any disturbance created by the jet would also be negligible. The conditions existing between sixty and one hundred thousand feet were considered, therefore, as a guide for this investigation.

This experiment was conducted at the University of Michigan supersonic wind tunnel in April, 1950.

The authors wish to express their appreciation for assistance and cooperation, to professor M. V. Morkovin who suggested the problem as outlined in Ref. 2., and acted as Faculty Advisor; Mr. L. C. Garby who aided in taking the shadowgraphs, and otherwise facilitated the program; Mr. C. E. Wittliff and Mr. N. Fidh whose help was invaluable during the tunnel operation.

EQUIPMENT AND PROCEDURE

Dimensional Analysis:

The problem of determining what happens to the normal force, drag, and moment of a body, making use of a side control jet, was first attacked by the use of dimensional analysis. (Ref. 3. or 4.). The chief advantage in the use of dimensional analysis is that it deals directly with the independent variables or dimensionless parameter of the problem without a complete solution being known. That is, the number of variable quantities may be reduced from n to (n - m) if n is the number of physical quantities, and m the number of fundamental units such as mass, length, time, and temperature. The use of dimensional analysis as a guide for experiments with models, such as undertaken in this analysis, is extremely valuable.

Since it is known that the normal force, drag, and moment of a body is directly connected to the pressure distribution over the body, it at once becomes apparent that body pressure (P_h) is the principle dependent variable. The problem now becomes one of determining all the so-called secondary, or independent, variables that characterize the flow and influence P_h. That is, a functional relationship must be found between P_h and these secondary variables. The composite flow for a given angle of attack is characterized by the following variables: (see list of symbols)

$$P_h,\ T_1,\ U_1,\ P_1,\ \mu_1,\ \rho_1,\ D,\ d,\ P_o,\ \rho_j,\ \mu_j,$$

$$U_j,\ T_o.$$

That is:

$$P_h = f(T_1, U_1, P_1, \mu_1, \rho_1, D, d, P_o, \mu_j, \rho_j, U_j, T_o)$$

Applying the theory of dimensional analysis to the problem and proceeding as outlined in Ref. 3 or 4, the thirteen variables (n) and four fundamental units (m) will give nine dimensionless parameters (n - m). This leads to

$$P_h/P_1 = f\left[\frac{\mu_1}{\mu_j}\right]\left[\frac{\rho_1 U_1 D}{\mu_1}\right]\left[\frac{P_o}{P_1}\right]\left[\frac{d}{D}\right]\left[\frac{\sqrt{\gamma P_1/\rho_1}}{U_1}\right]\left[\frac{\rho_j}{\rho_1}\right]\left[\frac{U_j}{U_1}\right]\left[\frac{T_o}{T_1}\right] \qquad (1)$$

This is not necessarily the only combination of dimensionless parameters that may be formed. However, any other such set of dimensionless numbers must be derivable from the one chosen here by multiplication or division with dimensionless numbers only. For example, a dimensionless parameter involving mass flux from the jet $\left[\frac{m_j}{\rho_1 D^2 U_1}\right]$, could become an independent parameter if desired. The experimental control of such a mass flux parameter, however, presented difficulties, so that it was not chosen as an independent parameter in the present analysis. Its dependence upon the chosen independent parameters is as follows:

$$\left[\frac{\pi}{4}\right]\left[\frac{d}{D}\right]^2\left[\frac{\rho_j}{\rho_1}\right]\left[\frac{U_j}{U_1}\right] = \frac{m_j}{\rho_1 D^2 U_1}$$

The number of parameters in equation (1) was reduced by considerations discussed below.

Considering equation (1) and the experimental facility for varying the eight independent parameters, the following

were neglected for the reasons given:

$\left[\frac{T_o}{T_1}\right]$ In order to vary T_o, high temperatures of jet air supply would be required to give an appreciable variation to this parameter. This was impractical; therefore no attempt was made to vary T_o. Before actually running the experiment T_o was investigated under simulated experimental conditions and found to be nearly constant. T_1 was affected only by atmospheric temperature and was also essentially constant. Therefore, the effect of this parameter was not considered.

$\left[\frac{\sqrt{\gamma P_1/\rho_1}}{U_1}\right]$ This parameter is the reciprocal of the wind tunnel Mach number, and as the investigation was made at one Mach number, this parameter was constant.

$\left[\frac{\rho_1 U_1 D}{\mu_1}\right]$ This parameter is the wind tunnel Reynolds Number based on the diameter of the body, and as only one body was investigated at a single Mach number, this parameter also could not be varied.

$\left[\frac{U_j}{U_1}\right]$ Supersonic speed is maintained in both the tunnel and the jet, and U_1 is constant. U_j is jet throat velocity and is equal to a_j, where a_j = constant x $\sqrt{T_o}$. As T_o was essentially constant; this parameter will not vary. Care was taken in the design that the smallest constriction in the air supply line to the jet was always larger than the jet throat area.

$\left[\frac{\rho_j}{\rho_1}\right]$ This parameter cannot be varied independently as ρ_j is a function of P_o from the equation of state, bearing in mind that T_o/T_1 is considered constant.

$\left[\frac{\mu_1}{\mu_j}\right]$ As the gas in both the tunnel and the jet is air, and T_o/T_1 is considered constant; this parameter will not vary.

As a result of the above considerations equation (1) reduces to:

$$P_h/P_1 = f\ (P_o/P_1)(d/D)$$

The dimensional analysis used above was developed for one configuration of the body. If we now introduce another configuration, by changing the angle of attack, the dimensional analysis would be the same with the same variables involved; except that now angle of attack (α) must be introduced as another independent parameter. Equation (1) then reduces to:

$$P_h/P_1 = f\ (P_o/P_1)(d/D)(\alpha) \qquad (2)$$

The parameters in equation (2) are all experimentally variable and directly measurable. This eliminated the necessity of any calculation, such as would have been required if another physical quantity (for example, mass flux from the jet) had been measured and P_o then determined from this measurement by the use of one-dimensional theory.

Model Design:

In considering the model design, it was assumed that an airborne craft flying at sixty to one-hundred thousand

feet, and making use of a side control jet (similar to the V-2 type power plant) might have the following characteristics:

(a)	Operational altitude	60,000 - 100,000 ft.
(b)	Control side-jet thrust	1,500 - 2,000 lbs.
(c)	Chamber pressure in side control jet	280 - 330 psi.
(d)	Exit velocity of side control jet	5,500 - 6,500 ft./sec.
(e)	Exit temperature of side control jet	3,000 - 4,000 degrees F.
(f)	Total propellant used by side jet	8 - 14 lbs./sec.
(g)	Ratio of jet throat diameter to body diameter	0.07 - 0.15

With these characteristics in mind a model was designed. This model consisted of a cone-cylinder combination with a total cone angle of 20° as shown in Fig. 1. Various dimensions of the model are shown on Fig. 2. This model was chosen for two reasons. First, because it was representative of the type of body in which a side control jet might be used; and second, because experimental results of pressure distribution on this type of body, having the same cone angle, were available (Ref. 5.). The diameter of the cylindrical portion of the body was chosen so as to avoid the possibility of tunnel choking. In this connection some concern was felt as to whether the side jet would add to the possibility of choking. Fortunately no choking occurred, even when the jet was started before the tunnel.

The use of a stagnation pressure chamber in the model to give a direct measurement of P_o was decided upon. This choice saved considerable work in obtaining P_o, as other methods proposed involved accurate metering of the air and measurement of T_o, from which P_o would then have to be calculated.

Compressed air from a constant pressure reservoir was fed into the body stagnation chamber through the sting as shown in Fig. 3. The compressed air was controlled and regulated by a throttling valve in the air supply line to give variations in P_o as desired. The air then issued through the nozzle into the supersonic stream of the tunnel.

Two interchangeable side jet nozzles were used. This limited the (d/D) parameter to only two values. One nozzle was straight with a diameter of 0.316". The other was a divergent nozzle of throat diameter of .150", an exit diameter of 0.316", and a 15° divergence angle.

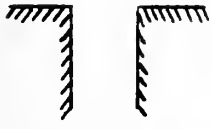

Straight Nozzle

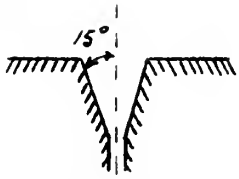

Divergent Nozzle

In order to vary the three independent parameters (d/D), (P_o/P_1), and (α), runs were made at $\alpha = 0°$ with the straight nozzle installed, at $\alpha = 14°$ with the straight nozzle installed, and at $\alpha = 14°$ with the divergent nozzle installed. An angle of attack of 14° was chosen as it was the greatest that could be obtained in the tunnel. This was considered desirable in order to determine if the side jet would induce separation at high angles of attack.

Because of the complications of the model construction a total of only seventeen orifices was available. These were located on the model to cover an area assumed to be in the region influenced by the jet. A removable, adjustable probe was available for investigations of static pressures at various locations around the model and at varying distances from the body as shown in Fig. 1. In addition, tufts were placed on the model during several runs to give a visual indication of the flow pattern about the model.

Supporting Instrumentation:

A schematic diagram of the location of the various instruments used is shown in Fig. 3. The pressure gage (previously calibrated), for measuring stagnation pressure in the model chamber, was located beside the compressed air supply throttling valve to facilitate throttling to desired stagnation pressures (P_o). Stagnation temperature (T_o) was measured in the compressed air supply line as close as possible to the model. This helped to minimize changes in stagnation temperature due to line losses in the air supply line. That portion of the air supply line exposed to the low temperatures in the tunnel was insulated with asbestos to prevent the low tunnel temperatures from affecting T_o. As a result of these precautions, stagnation temperature of the air supply was practically constant, at the point measured, throughout the experiment.

Static pressures from the seventeen static pressure orifices were read on the manometer board as shown in Fig. 3.

to give values of P_h. In addition, two static flow pressures were read at points in the tunnel fourteen inches upstream of the test section centerline. These gave values of (P_1).

Experimental Procedure:

Photographs of the manometer board were taken on all runs, and in most cases Schlieren pictures were taken simultaneously with those of the manometer board. This was done to give instantaneous comparison of Schlieren and pressure data for each run. For comparison with the Schlierens, several shadowgraphs were made. No manometer pressures were available on these runs as the shadowgraphs had to be made in complete darkness.

Data Reduction:

Data was reduced as shown in the section on "Sample Calculations" and tabulated in Table I. The data from several runs were not reduced or tabulated because, during these runs, either P_o was varying or the manometer board had not steadied down at the time the photographs were taken. The data in Table I. were then plotted in Figs. 4-12, where P_h/P_1 vs P_o/P_1 was plotted for the various static pressure orifices. In determining the effect of the changing pressures on the body, resulting from the introduction of the side jet, the change in pressure, $\Delta P_h/P_1$, was integrated in an approximate manner over the body (Figs. 13 and 14). The change in pressure $\Delta P_h/P_1$ was the change from no jet to maximum jet. This procedure is outlined in "Sample Calculations". This inte-

gration gave an approximate change in normal force, drag, and moment about the center of gravity resulting from the side jet.

RESULTS AND DISCUSSION

In an actual airborne body having characteristics similar to those outlined in "Equipment and Procedure", the P_o/P_1 ratio would probably vary from 150 to 300. The P_o/P_1 ratios obtained in this investigation varied from zero to 58.0. The results of this investigation, therefore, will show a trend toward what might be expected in an actual airborne body.

Variations of pressure ratio (P_h/P_1) over the body at each static pressure orifice (or tap) with variations of P_o/P_1, α, and d/D are shown in Figs. 4-12.

General Flow Discussion:

Figs. 15, 16, 17 show the approximate areas on the body affected by maximum jet in terms of areas of low pressure (suction) and high pressure as compared to the pressure distribution with no jet acting. These were drawn from Figs. 4-12 and, while only approximate, give a general indication of the effects of varying the angle of attack and the d/D parameter.

Figs. 15, 16, and 17 all show three general pressure zones: (1) a narrow band of high pressure on the outer edges of the area affected by the jet. This band might possibly be associated with the jet shock as it forms around the body. (2) A region of suction where the jet apparently has a "pump" effect and creates a low pressure area extending from just forward of the jet exit to the vicinity of taps 4 and 5.

(3) A high pressure zone on the tail of the body probably due to the return of a portion of the jet flow to the tail (discussed below).

There is strong evidence that after the jet leaves the body at the jet exit it returns to the body near the tail. This was not expected as jet flow from a wall orifice normal to a subsonic tunnel flow does not return to the wall (Ref. 1). It is felt that the return of the jet to the body in the present investigation is due to the three dimensional aspects of the flow. Schlieren photographs Figs. 18 and 19 show a definite line of discontinuity in the jet flow which appears to be returning to the after portion of the body. This is partially confirmed by run numbers 4-22-16, 4-24-1, and 4-24-17 where a probe was located near the top of the body at three different positions between the jet and the tail. In run number 4-22-16, with the probe closest to the jet, strong vibrations of the probe were noted. These vibrations decreased when the probe was moved aft in run number 4-21-1. With the probe still further aft (just forward of the base), it was noted that the probe was pressed down against the body and did not vibrate at all.

In addition, tufts placed on the body in various locations in runs 4-22-7, 4-22-15, and 4-22-16 indicated that behind the jet, flow was generally upward away from the body in the vicinity of taps 3 and 4, while flow was again parallel to the body in the neighborhood of taps 5 and 6, as shown in Fig. 15a.

From these observations it seems likely that the jet, after leaving, returns to the body. This return to the body appears to be a function of P_o/P_1 as evidenced by the rearward movement of the high pressure zone on the tail with increasing P_o/P_1 (to be discussed later). It is also apparently a function of the length of the body.

In addition to the return of the jet flow to the tail, there appears to be an unsteady condition in the jet flow, as evidenced by the rather wide scatter of plotted points for tap No. 6 as shown in Figs. 4 and 7.

A comparison of Figs. 15, 16, and 17 with the Schlieren photographs (Figs. 18 and 19) shows a close correlation between shock locations and flow patterns of the photographs with the pressure zones of Figs. 15, 16, and 17. Fig. 15a. shows a typical sketch of a Schlieren photograph at zero angle of attack with the straight nozzle installed. Comparing Fig. 15. with Fig. 15a. it can be seen that the small high pressure zone ahead of the nozzle corresponds to the shocks produced ahead of the jet. In this area one would expect to find high pressures due to the shock. The large suction zone in the vicinity of the jet on Fig. 15. is indicated by the tuft directions just behind the jet (Fig. 15a.). The return of the jet to the tail (discussed above) is evidenced by a line of discontinuity returning to the tail (Fig. 15a.). This flow return would also account for the high pressures on the tail, as the jet flow, although expanding rapidly, would

probably still be of higher pressure where it strikes the tail than the pressures over this region when no jet was acting.

α Effect:

Comparison of Figs. 15. and 16. revealed that at $\alpha = 0^\circ$ a larger area on the model was affected by the suction from the jet than at $\alpha = 14^\circ$. The same occurs in the high suction zone just behind the nozzle. For the high pressure zone just forward of the nozzle, areas of approximately the same size were affected. The high pressures felt near the tail in the vicinity of tap number 6 are approximately the same for $\alpha = 0^\circ$ and $\alpha = 14^\circ$. This seems to indicate that there will be a greater body normal force developed from the jet action at $\alpha = 0^\circ$ because of the larger suction area. This is verified by the results of the pressure integration to be discussed later.

Nozzle Effect:

In comparing Figs. 16 and 17 it should be remembered that for the divergent nozzle, due to its smaller throat area, mass flux through the jet is approximately 25% of that through the straight nozzle for a given P_o/P_1 value. Figs. 16 and 17 give a comparison of the approximate regions of suction and pressure over the body for the straight nozzle and the divergent nozzle, respectively; both at a 14° angle of attack.

From Figs. 16 and 17 it is noted that for the divergent nozzle (Fig. 17) the high pressure zone in front of the nozzle has narrowed considerably. The suction zone from the

divergent nozzle seems to extend over a larger area than for the straight nozzle, and is of lower overall intensity. The high pressure area near the tail is of greater area and greater magnitude for the divergent nozzle. From this it would seem that the divergent nozzle will not have as great an effect on the body normal force as will the straight nozzle. Since the divergent nozzle has lower mass flux and less shock effect than the straight nozzle it is possible that a more logical result might be shown by the use of mass flux as a variable. Schlieren photograph, Fig. 20, shows a stronger jet shock than Fig. 21. where less mass flux is being ejected.

A rather peculiar phenomenon seems to occur at taps 10 and 13 (Figs. 16 and 17) where the pressures reverse themselves when the nozzle is changed from straight to divergent. It is rather difficult to explain this, but it is believed that the side component of velocity from the divergent nozzle, in some way affects the mixing zone and narrows down the suction zone in the vicinity of the jet. Tap number 10 would now lie in the band of high pressures just outside the suction zone, as shown in Fig. 17.

Further Details of the Flow:

The pressure distribution over the body for several of the curves in Figs. 4-12 show reversal of trends as P_o/P_1 increases. A rather wide scatter of plotted pressures may also be noted for several runs at higher P_o/P_1. Figs. 4, 5, and 6 show that the only taps that reverse their trend

with increasing P_o/P_1 are numbers 2, 5, and 10. The reversal of number 2 might be accounted for by the forward movement of the shock formed in front of the jet. As P_o/P_1 was increased, number 2 might lie eventually in the suction zone created by the jet, thus accounting for its reversal in trend. The reversal of number 5 seems to indicate that as P_o/P_1 increased the high pressure zone on the tail moved further aft. Number 10 shows a rather sharp drop for high P_o/P_1 values, possibly accounted for by the fact that the suction zone from the jet moves rather rapidly around the body in the vicinity of the jet, for higher values of P_o/P_1.

Referring now to Figs. 7, 8, and 9, tap number 2 shows a considerable scatter at high P_o/P_1 values. As number 2 shows higher pressures with the jet acting than for no jet ($P_o/P_1 = 0$), number 2 evidently lies in the area just behind the shock produced by the jet, where a more or less turbulent region exists as shown by the Schlieren photograph, Fig. 20. The scatter of tap number 6 is probably due to the unsteady flow conditions produced by the jet. This unsteadiness is evidently felt more strongly where the jet returns to the body, as discussed previously.

Schlieren photographs Figs. 22 and 23 indicate that a shock is present in the jet flow just outside the jet exit. The shock would mean an increase in static pressure in the jet flow. This might partially account for the high pressures at tap number 6 where the flow has returned to the body.

The shock configuration in the jet flow is of the following general appearance:

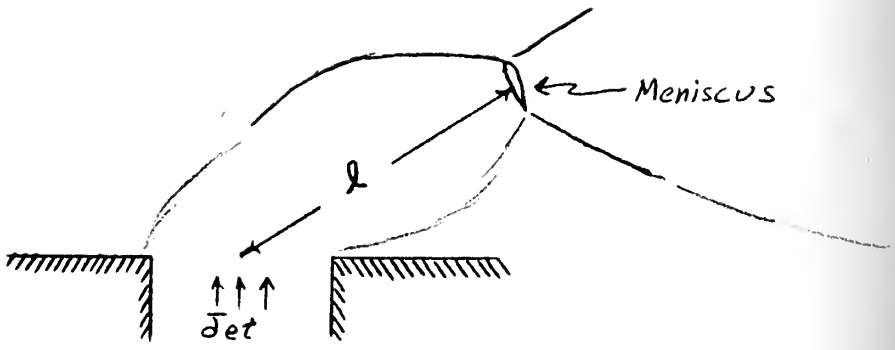

This may also be clearly seen in Fig. 24. The configuration above is similar to that of Fig. 24a. except that here it is deflected by the tunnel flow. Variation of the meniscus length, l, with P_o/P_1 and with mass flux is discussed in Appendix B.

For an angle of attack of 14° a plot of P_h/P_1 vs. x for $P_o/P_1 = 0$ (where x is the distance in inches along the top of the body measured from the shoulder) is shown in Fig. 26. This plot does not agree either with theoretical or experimental results of Ref. 5 where the variation of the coefficient of pressure (Cp) along the body was found to increase linearly with x. Cp was recomputed in terms of P_h/P_1 and plotted on Fig. 26 to show the comparison. The investigation undertaken in Ref. 5 was made at angles of attack from zero to ten degrees on a cone-cylinder body with a cone angle of 20°. Variations from this linearity, as shown in Fig. 26 indicate that, for angles of attack

greater than one half the cone angle, this linear variation may no longer exist. This suggests the possibility of further investigations concerning this variation.

A possible cause of this non-linearity may be the thick boundary layer build up along the top of the body as shown by Fig. 25. This could, because of viscosity, alter the theoretical results in a manner similar to the results of Ref. 6, where viscous effects introduced a considerable variation from the theoretical predictions.

Normal Force, Moment About the Center of Gravity, and Drag:

Changes in normal force, drag, and moment about the center of gravity, due to the action of the side jet, and their respective coefficients ΔC_N, ΔC_D, and $\Delta C_{M_{CG}}$ were determined by approximate integration as outlined in "Sample Calculations". These results are tabulated in Table II and plotted in Figs. 27, 28, 29. The point of application of the resultant normal force is also shown on Figs. 27, 28, 29. From a consideration of the above figures, it appears that the point of application of the resultant normal force does not vary greatly with changes in angle of attack with the straight nozzle installed. However, when the straight nozzle is replaced by the divergent nozzle a large forward movement of this point of application was noted. This forward movement caused a reversal in sign of the moment coefficient ($\Delta C_{M_{CG}}$).

These values of the resultant normal force and moment about the center of gravity will be affected by the length of the body. If the body were shortened by removal of

section E, (Figs. 27, 28, 29) the upward resultant body normal force would be much greater, and its point of application moved considerably. This would also increase $\Delta C_{M_{CG}}$ in a negative sense. Conversely, if the body were lengthened, the downward normal force on the after part of the body would decrease the upward resultant normal force and also decrease the $\Delta C_{M_{CG}}$ in a negative sense. In the three configurations investigated ($\alpha = 0^\circ$, 14° for the straight nozzle, and $\alpha = 14^\circ$ for the divergent nozzle), the resultant body normal force is in the same direction as the jet flow. This indicates that the jet is acting as a pump creating a low pressure area on the body about the jet, thus giving a body normal force component directly opposing the jet thrust. In this investigation, the maximum body normal force component is approximately five percent of the jet thrust (see "Sample Calculations). Therefore, the nominal jet thrust will be decreased by about five percent due to the change in pressure distribution over the body caused by the jet.

With the straight nozzle installed, ΔC_D increased with angle of attack. At $\alpha = 14^\circ$ the divergent nozzle gave a lower ΔC_D than the straight nozzle. This seems to be in accord with the logic of the situation, as more mass flux and hence more disturbance was introduced by the straight nozzle, and one would normally expect this to cause greater drag.

This investigation was conducted with the thrust of the jet, acting at the center of gravity, tending to decrease the angle of attack. It is likely in maneuvering a body in

actual flight, that the opposite effect will be encountered when the jet will be used to increase the angle of attack. In this latter case, however, the change in normal force resulting from alterations in pressure distribution due to the presence of the jet will, from the above considerations, again directly oppose the jet thrust.

CONCLUSIONS

As a result of this investigation, the following conclusions may be drawn:

1. Although a complex mixing and flow pattern results from the side jet, no stall develops even at a 14^{0} angle of attack.

2. The "pump" effect of the side jet opposes the nominal jet thrust by a maximum of approximately five percent of the thrust.

3. Flow from the side jet returns to the body near the tail; thus hot jet gases might cause damage to any tail surfaces installed.

4. The magnitude of the change in normal force due to the side jet is a function of the length of the body.

5. The effect of the side-jet is felt on a curved triangular section of the body having its apex just forward of the side-jet and extending to the tail.

6. The divergent nozzle with a smaller mass flux does not have as great an effect on normal force as the straight nozzle.

7. The effect of the side-jet is to increase drag in all cases considered.

8. A moment about the center of gravity is induced by the effect of the side-jet, but this again is a function of the length of the body.

9. It is possible that more logical results might have been obtained if mass flux from the jet were considered as an independent variable.

RECOMMENDATIONS

The following recommendations are made:

1. That smoke be ejected with the air from the side-jet to give a visual interpretation of the flow.

2. That higher P_o/P_1 values be investigated to correspond to those that might be encountered in actual flight.

3. That the parameter T_o/T_1 be varied independently to determine the effect of the hot jet gases.

4. That the tunnel Mach number be varied independently.

SAMPLE CALCULATIONS

Data Reduction:

Original data taken from the manometer board pictures was reduced according to the following equations:

$$P_h = P_M - (\overline{P_R} - \text{Gage})$$

$$P_1 = P_{M_1} - (P_{R_1} - \text{Gage})$$

where

P_M is the manometer board reading for the various orifices (Nos. 1 through 17).

$\overline{P_R}$ is the average of the four reference level readings shown on the manometer board (Fig. 29a).

Gage is the absolute pressure of $\overline{P_R}$, read in millimeters of mercury and converted to inches of mercury for each run.

P_{M_1} is the manometer board reading for the static floor orifice.

P_R is the reference level reading on the manometer board for the static floor orifice.

As a specific example consider run 50-4-22-2. The manometer board for this run is shown in Fig. 29a. From Fig. 29a

$$\overline{P_R} = 7.40"$$

$$\text{Gage} = .045" \text{ Hg. (Not shown)}$$

$$P_M = 11.71 \text{ for orifice No. 1}$$

Therefore $P_h = 11.71 - (7.40 - .045) = 4.355"$ Hg.

Similarly $P_1 = P_{M_1} - (P_{R_1} - \text{Gage})$

$$P_1 = 11.22 - (7.23 - .045) = 4.035" \text{ Hg.}$$

For run 4-22-2 P_o = 80 psig. Corrected for Gage calibration (Fig. 29a)

P_o = 192.66" Hg. (Corrected for temperature and atmospheric pressure)

Therefore $P_o/P_1 = \frac{192.66}{4.035} = 48.1$

$P_h/P_1 = 1.080$

No correction for parallax was made as the parallax correction cancelled in the P_h/P_1 computations, and as P_o was only read to $\pm$.5 lbs. it was not considered in the P_o/P_1 computations.

Integration:

A sample of the integration for normal forces is shown in Fig. 13. and 14. Here $\Delta P_h/P_1$ for each orifice is plotted, where $\Delta P_h/P_1$ is the difference between the P_h/P_1 for maximum P_o/P_1 and the P_h/P_1 for $P_o/P_1 = 0$. Curves of $\Delta P_h/P_1$ were then plotted as shown on Fig. 13. for $\theta = 0°$, $45°$, $90°$, $135°$, and $180°$. In some case extrapolation of these curves was necessary. The body was then divided into 5 one inch sections as shown on Fig. 13. and the values of $\Delta P_h/P_1$ plotted as on Fig. 14. for Station "C". These values were then integrated as shown on Fig. 14. by taking $\Delta P_h/P_1 \times \cos\theta$ over one half the body as shown on the upper plot on Fig. 14. This area was then proportional to the normal force. From the dimensions of the integration;

Normal force in lbs. at station C = (.1) x (Total Area) x (P_1 in lb/in^2)

N = (.1)(Area)(.48) = (.048)(Area)

N = (.048)(6) = .288 lbs.

Similarly, Drag was computed by taking (resultant normal force)$(\sin\alpha)$ + $\left[(\Delta P_h/P_1)_{base}\right]\left[\cos\alpha\right]$. Here an assumption

was made that $\Delta P_h/P_1$ on the base was a constant value over the base of the same value as shown for tap No. 7. This was necessary as No. 7 was the only orifice giving base pressures. The resulting drag values should therefore be definitely considered as approximate in nature.

The above procedure was done at each of the five 1 inch sections and results plotted as shown on Figs. 27, 28, 29. Assuming that the center of gravity of the entire body was at the jet, $C_{M_{CG}}$ was then computed and also plotted on Figs. 27, 28, 29.

C_N, C_D, and $C_{M_{CG}}$ were computed from the following equations

$$C_N = N/qS$$

$$C_D = D/qS$$

$$C_{M_{CG}} = M/qSc$$

where

$q = \gamma/2\, P_1\, M_1^2 = 5.4$ lbs./in.^{2}

S = cross sectional area of body = π sq. in.

c = diameter of body = 2 inches.

and D = forces in pounds

M = moment in inch pounds

Thrust Computation:

The equation for the nominal thrust of a rocket is:

$T = \dot{m}\, v_e + (P_e - P_a)\, A_e$ Ref. 7 p. 10.

where

T = thrust in pounds

$\dot{m}$ = mass flux in slugs/sec.

v_e = effective exit velocity ft./sec.

P_e = exit pressure in lbs./ft.^{2}

P_a = tunnel pressure in lbs./ft.^{2}

A_e = Area of nozzle exit in sq. ft.

Assuming that the throat of the straight nozzle is at the exit this gives for maximum P_o:

m = .00527 slugs/sec.

v_e = 1138 ft./sec. = speed of sound at throat

$P_e = (.5283 \times P_o) = (.5283 \times 105) = 55.5$ lbs./in.^{2} = 7990 lb/ft^2

P_a = 2.25 lb/in^2 = 324 lb/ft^2

$A_e = (.316)^2 \pi/4 \times 1/144 = .000498$ ft.^{2}

Therefore

Thrust = (.00527)(1138) + (7990 - 324)(.000498)

T = 6 + 3.72 = 9.72 lbs.

From pressure integration over the body

N = .518 lbs. Fig. 27.

N/T = .518/9.72 = .0533

or N is approximately 5% of the thrust but in the opposite direction.

Computation of m_j (mass flux in slugs/sec. from the jet)

$$m_j = \rho AV = \frac{\gamma VAP}{a^2} = \frac{\gamma MAP}{a} \quad \text{as} \quad \rho = \frac{\gamma P}{a^2}$$

at throat M = 1

$$m_j = \frac{\gamma A_t P_t}{a_t} = \frac{\gamma A_t (.5283 P_o)}{\sqrt{\gamma R \left(\frac{2}{\gamma+1} T_o\right)}}$$

$$m_j = \frac{.5283\,\gamma\,A_t\,P_o'}{\sqrt{(\gamma R)\left(\frac{2}{\gamma+1}\,T_o\right)}}$$

$$m_j = \frac{(1.4)(.5283)\,A_t P_o}{\sqrt{\frac{2\gamma R}{\gamma+1}\,T_o}} = \frac{.0165\,A_t P_o}{\sqrt{T_o}}$$

$$m_j = \frac{.0165\,A_t P_o}{\sqrt{T_o}} \quad \text{slugs/sec.}$$

$T_o = 528°R$

$m_j = .00078\,A_t P_o$ slugs/sec.

for straight nozzle $m_j = (.0000564)(P_o)$ slugs/sec.

for divergent nozzle $m_j = (.0000187)(P_o)$ slugs/sec.

APPENDIX A.

Included herein is a description of the supersonic wind tunnel at the University of Michigan Aeronautical Research Center and a presentation of aerodynamic characteristics and physical dimensions necessary for the planning of wind tunnel tests.

I. General Configurations

The wind tunnel is an intermittent vacuum type with its operating potential resulting from the pressure differential between air stored at atmospheric pressure and the low pressure of an evacuated tank. A diagrammatic sketch of the tunnel components showing their relative location is shown in Figure 1.

This figure shows the 24,000 cu. ft. fabric storage bag, its outlet to the tunnel channel, the test section, the diffuser, the master valve, and outlet into the 12,000 cu. ft. vacuum tank. The air is drawn from the vacuum tanks by the vacuum pump, forced through the surge tank, through the percipitron filter and into the storage bag. A separate circuit continuously draws air from the front end of the storage bag through a drier utilizing activated alumina and back into the storage bag.

II. Tunnel Channel

The tunnel channel consists of the nozzle region, the test section, and the diffuser. The test Mach number is

obtained by the use of removable nozzle blocks. These blocks are 56" in length and span the 8" width of the tunnel. The anticipated test Mach numbers are 1.5, 2, 2.5, 3, 3.5, and 4, of which the 1.5, 2, 3, and 4 are presently available.

The test section of the tunnel is of uniform cross section, uncorrected for boundary layer, 8" wide and 13" deep with an overall length of 45". The test section side walls are fitted with optically ground windows 16" in diameter for Schlieren photograph and visual observation. The diffuser is of the immovable body type. The tunnel channel is shown in Figure 2.

III. Aerodynamic Characteristic Within the Test Section

Plotted in Figure 3. are the static pressure, temperature, dynamic pressure, density, and Reynolds Number as a function of the test section Mach number. Shown in Figure 4. are the Mach number and pressure distributions at Mach 1.9, the Mach number at which these tests were run. Figure 5. is a plot of tunnel run time as a function of the time required to evacuate the tanks.

A SKETCH OF COMPONENT PARTS OF TUNNEL

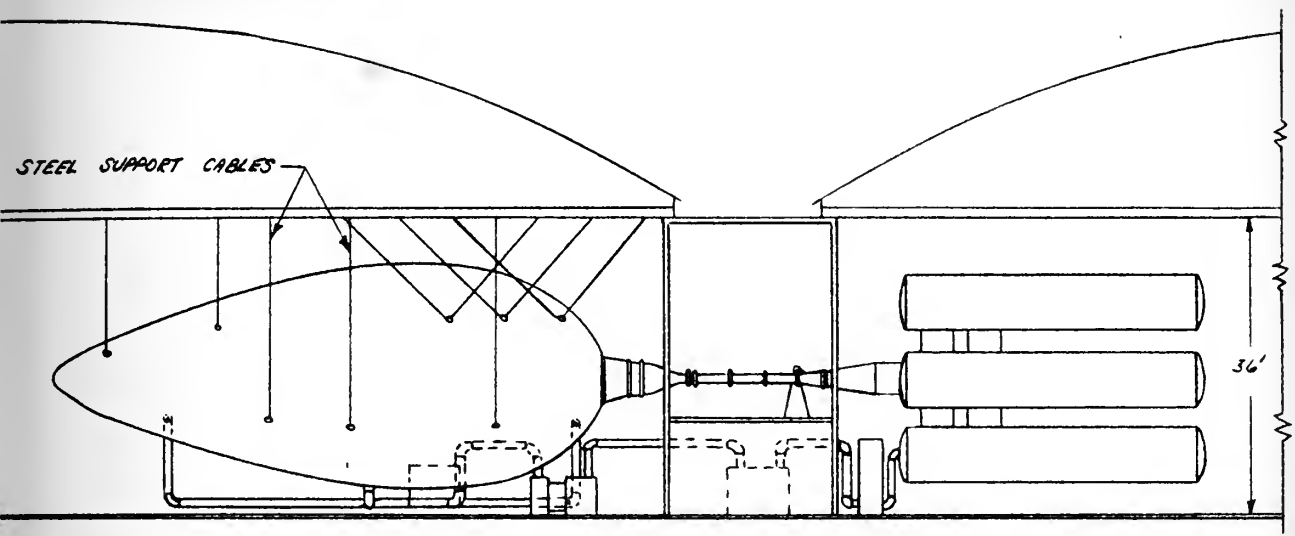

SECTION A-A

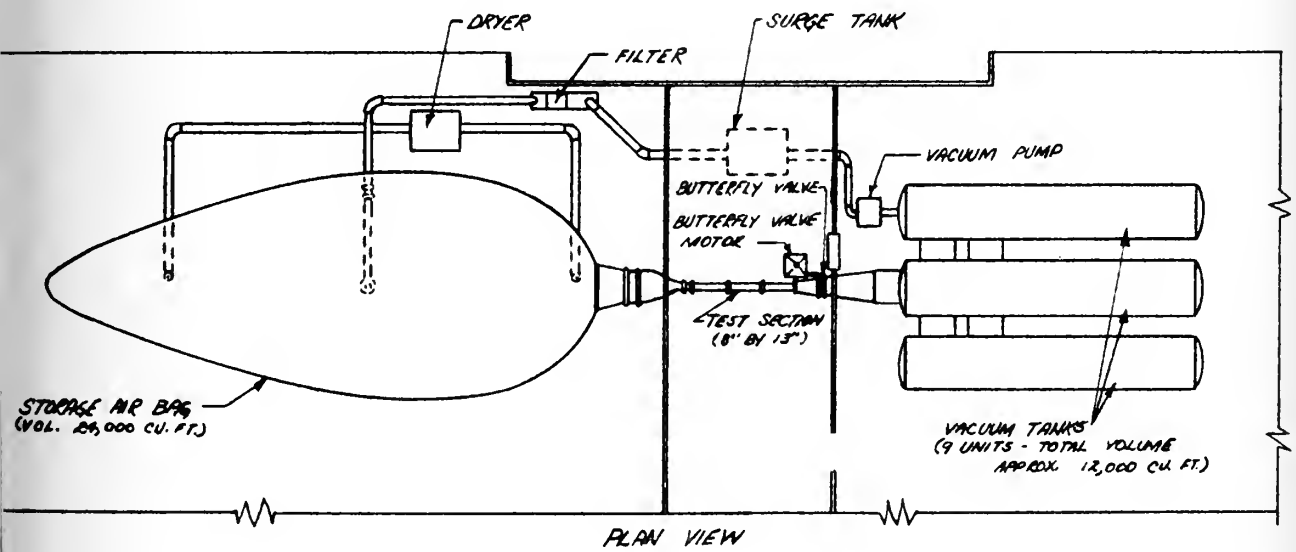

PLAN VIEW

FIGURE 1

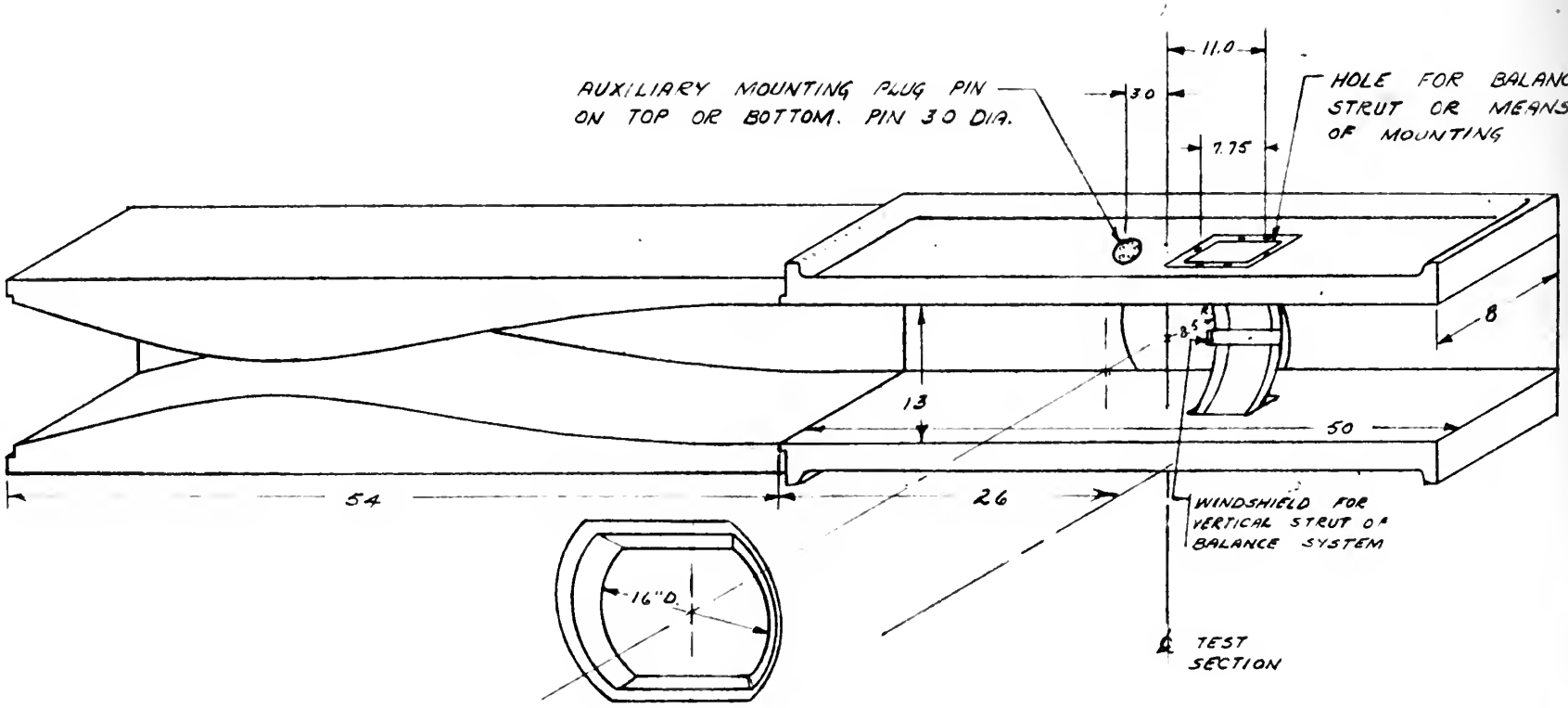

SKETCH OF NOZZLE - TEST SECTION REGION OF AIR CHANNEL

FIGURE 2

AERODYNAMIC CHARACTERISTICS
1 FT SECTION AS A FUNCTION OF MACH NUMBER

FIGURE 3

T_0 = 59° F = 518.6° R

P_0 = 2116 P.S.F.

ρ_0 = .002378 SLUGS/FT.^{3}

LENGTH BODY = 1 FT.

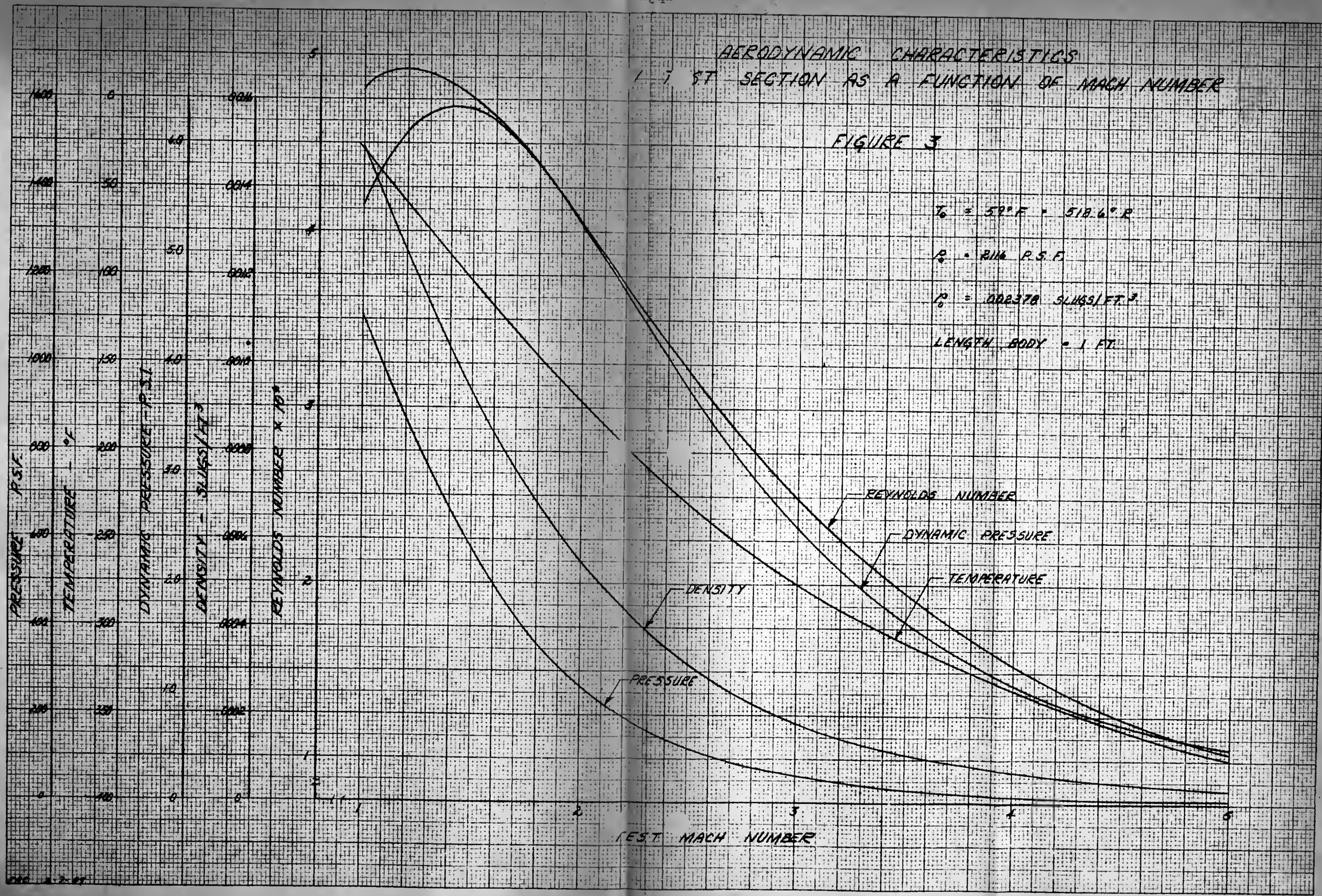

UNIVERSITY OF MICHIGAN SUBSONIC WIND TUNNEL CALIBRATION

MACH NUMBER 1.90

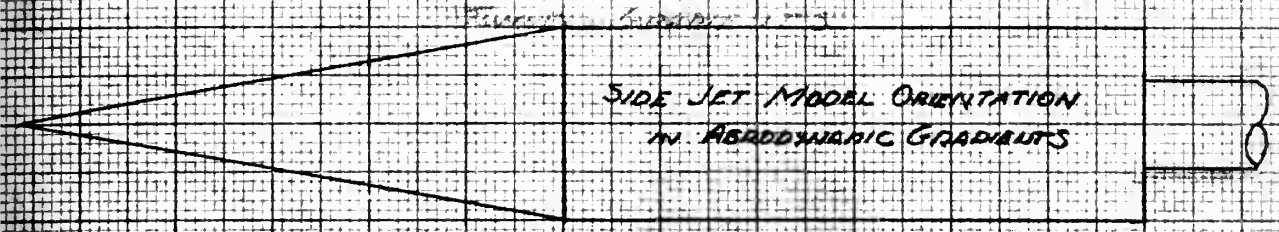

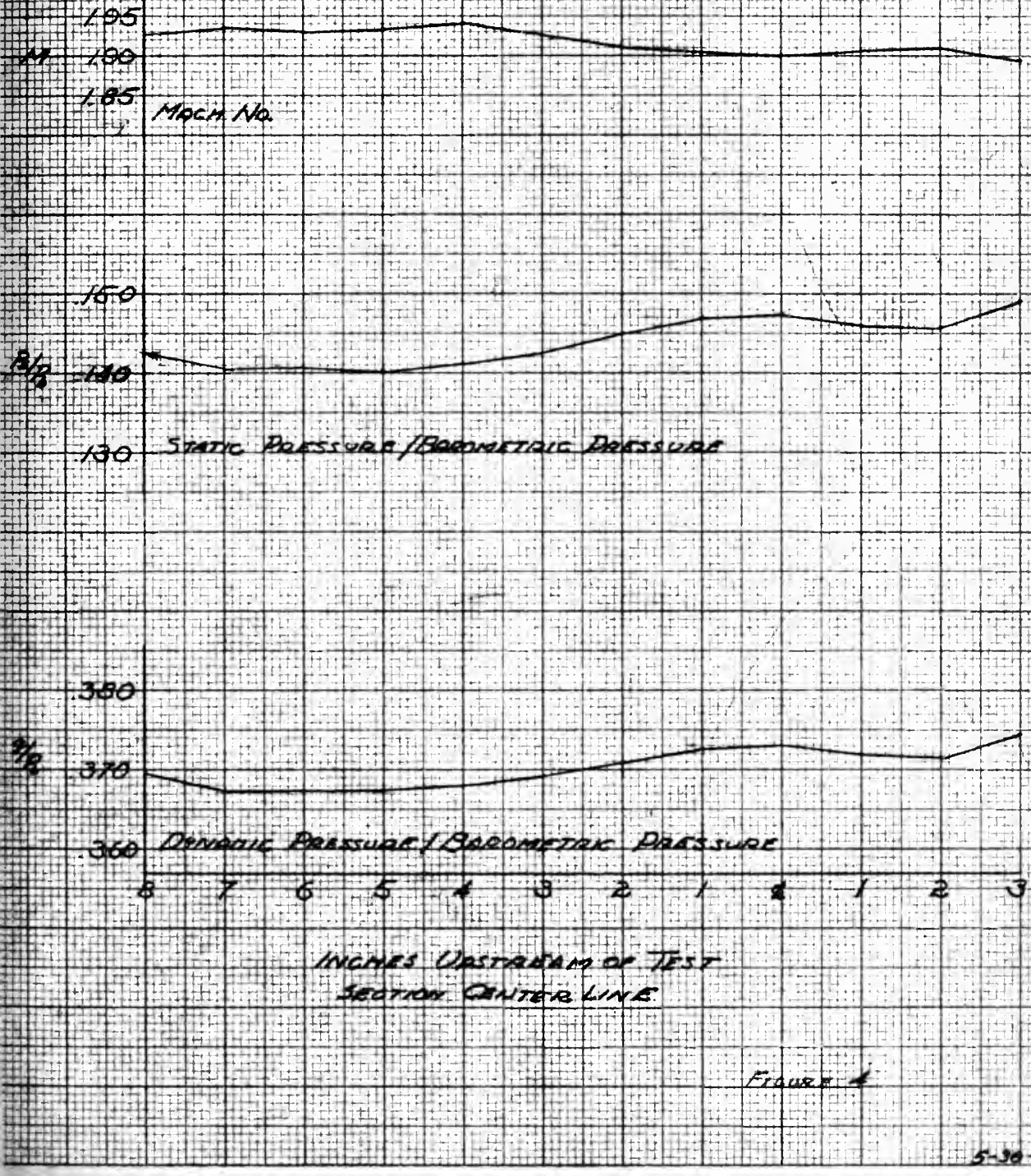

FIGURE 4

5-30-50

MAXIMUM TUNNEL RUNNING TIME VERSUS PUMPING TIME M = 1.90

FIGURE 5

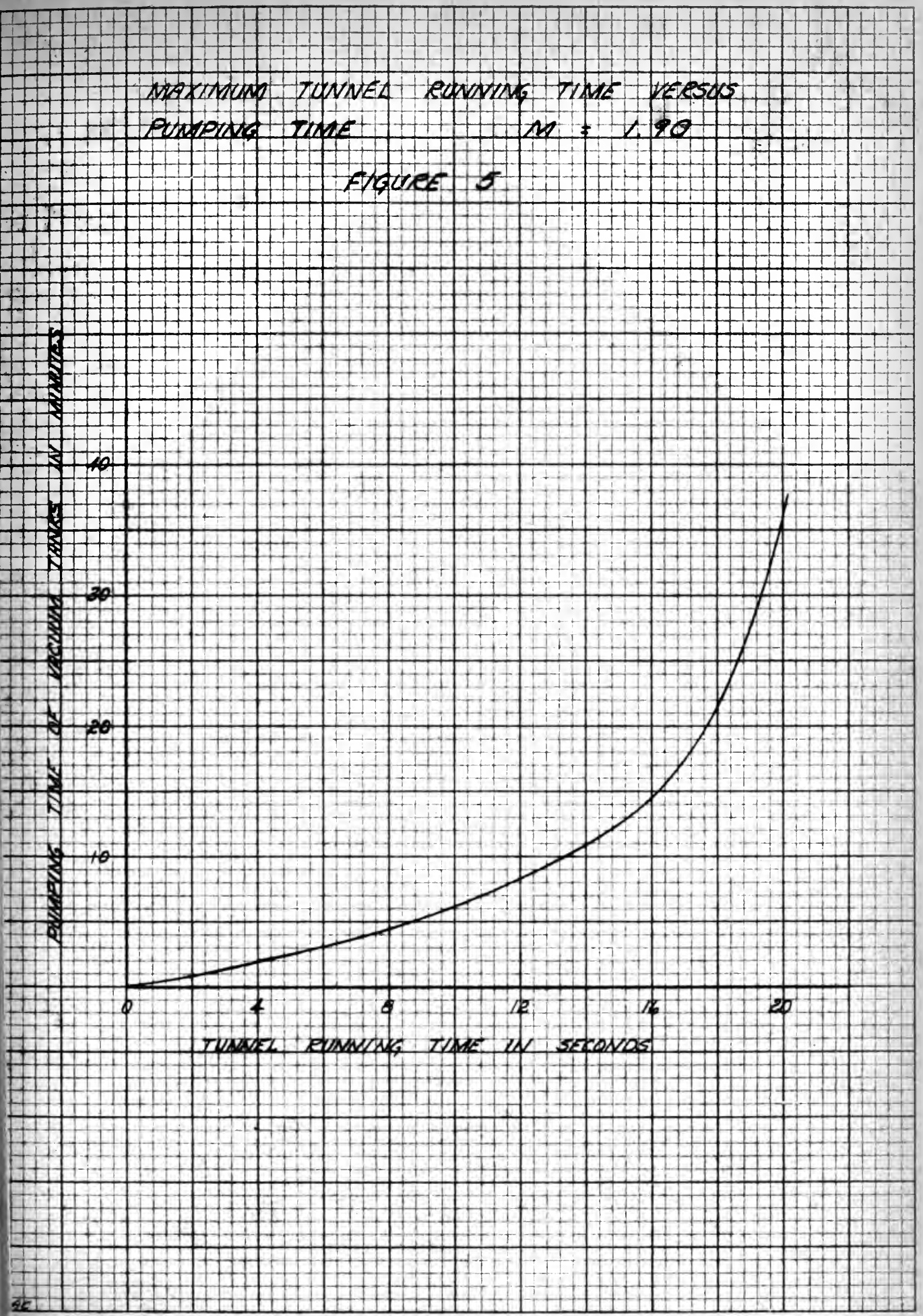

APPENDIX B.

Apparent Linearity of Meniscus Length with P_o/P_1 and m_j.

Fig. 30. shows a plot of meniscus length (l) (see sketch p. 19) vs. P_o/P_1 for $\alpha = 0^\circ$ and 14°, straight nozzle; and for $\alpha = 14^\circ$, divergent nozzle as tabulated in Table III. This distance l was measured from the centerline of the jet exit to the meniscus of the jet shock, which is formed in the jet flow, and discussed under "Results and Discussion".

Referring to Fig. 30. there appears to be a linear relation between the location of this shock meniscus and the P_o/P_1 values.

Fig. 31. shows a similar relation between meniscus length (l) and m_j as tabulated in Table IV. Here again a linearity seems to exist.

APPENDIX C.

Fig. 24. is a shadowgraph of the model with the side jet operative. The model is at a 14° angle of attack. A peculiar phenomenon is present at the jet exit. Here the jet exit, although flush with the body on the actual model, appears to be sunken and to have shoulders on either side. This is an excellent although extreme example of the principle of the shadowgraph as described in Ref. 8, pages 98 and 99. As stated in Ref. 8, "a density gradient in the flow causes a deflection of the rays in the direction of that gradient". In the shadowgraph, referring to the "sunken" appearance of the jet, the gradient is very strong from the low pressure area outside the jet to the comparatively high pressures in the jet itself. This will cause a downward deflection of the light rays passing through the jet and will account for the "sunken" effect of the jet.

Referring now to the "shoulders" on the jet exit the opposite is true. The transition from low pressure on the body just around the jet exit to the high pressures in the jet as it expands outside the body gives a strong upward pressure gradient. This causes the light rays to be reflected upwards and accounts for the "shoulders" shown in Fig. 24.

REFERENCES

1. NACA T.N. 1615. "Investigation of the Penetration of an Air Jet Directed Perpendicularly to an Air Stream" by E. F. Callaghan and R. S. Ruggeri June 1948.
2. "Analysis of Schlieren Photographs of the Pressure-Pulse Technique" by M. V. Morkovin and E. Migotsky. University of Michigan Wind Tunnel Memorandum No. 60, January 4, 1949.
3. "Dimensional Analysis" by P. W. Bridgeman. Yale University Press, New Haven, Connecticut 1922.
4. "Handbook of Engineering Fundamentals" edited by O. W. Eshbach. John Wiley and Sons, Inc. New York 1936. Eleventh Printing.
5. "The Experimental and Theoretical Pressure Distribution and Normal Force of a Cone-Cylinder Configuration at a Mach Number of 1.93" by W. S. Dorrance. University of Michigan Engineering Research Institute EMB-10 of January 20, 1949.
6. NACA T.N. 2044 "Pressure Distribution and Some Effects of Viscosity on Slender Inclined Bodies of Revolution" by H. J. Allen March 1950.
7. "Mathematical Theory of Rocket Flight" by Rosser, Newton and Gross. McGraw-Hill Book Co. Inc. New York 1947.
8. "Aerodynamics of a Compressible Fluid" by Liepmann and Puckett. John Wiley and Sons, New York, 1948. pp. 98-99.

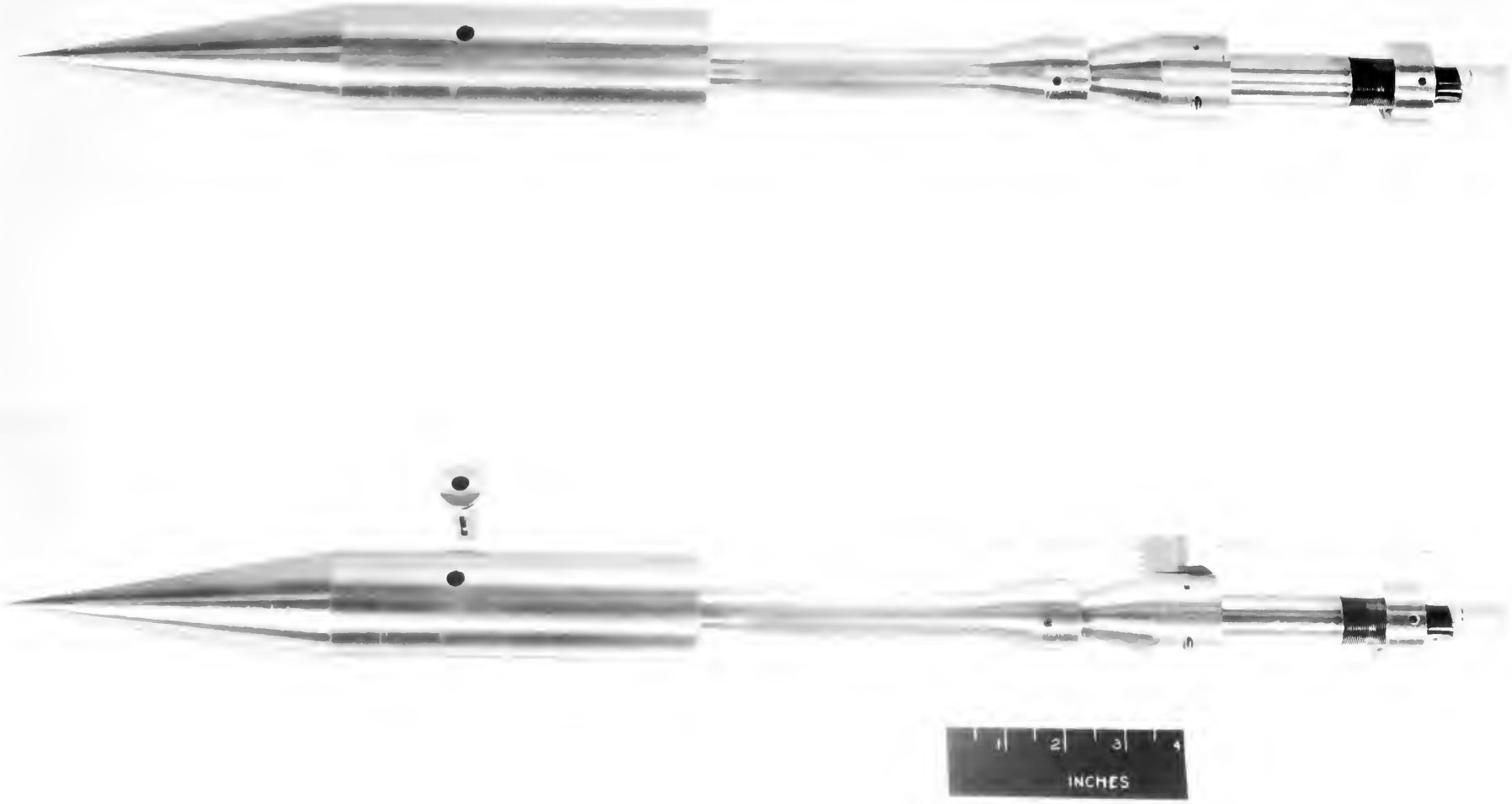

FIG. 1.

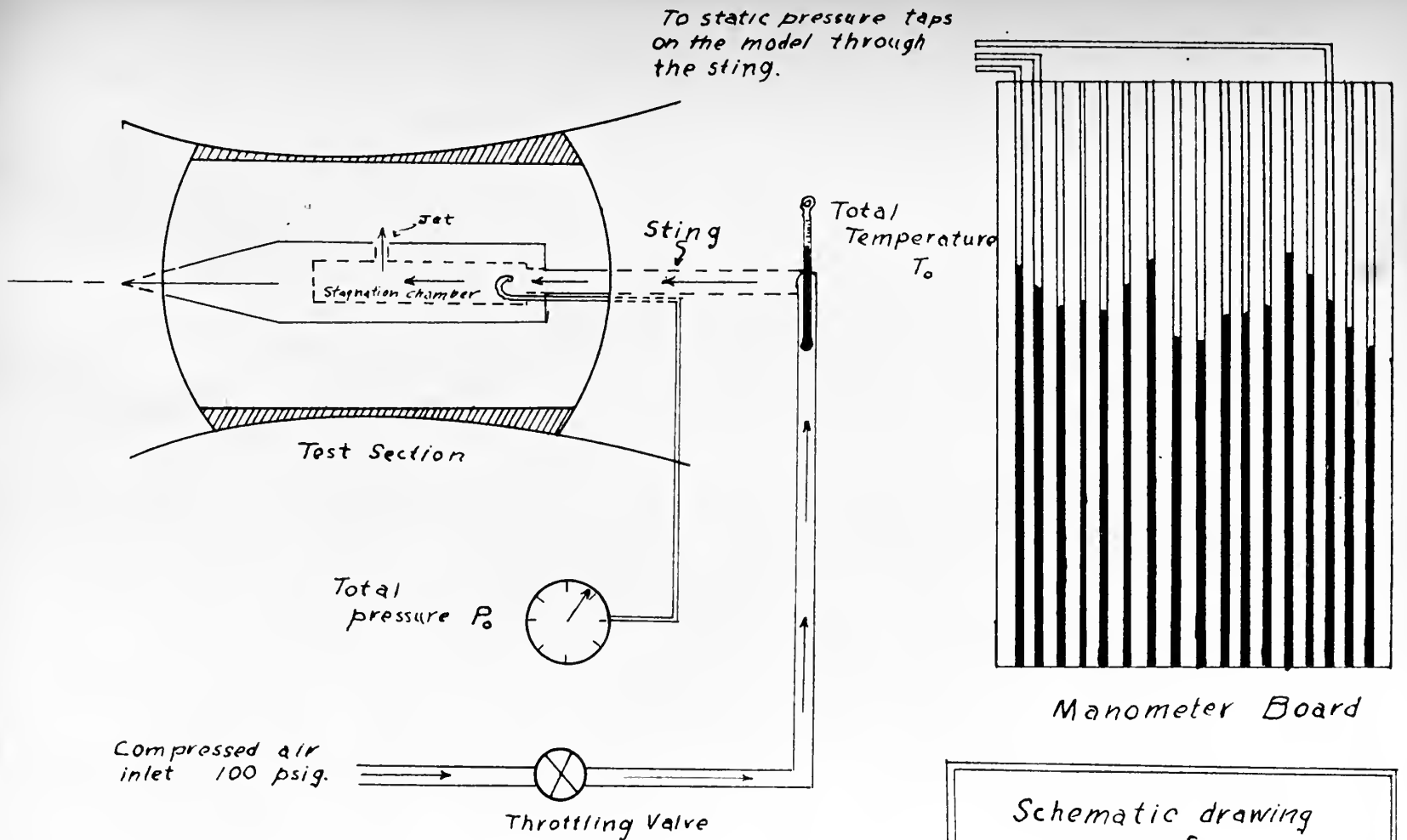

Schematic drawing of Test Set-up FIG. 3.

Change in P_4/P_1
With Varying P_2/P_1
$\alpha = 0°$ Straight Nozzle
Fig. 4.

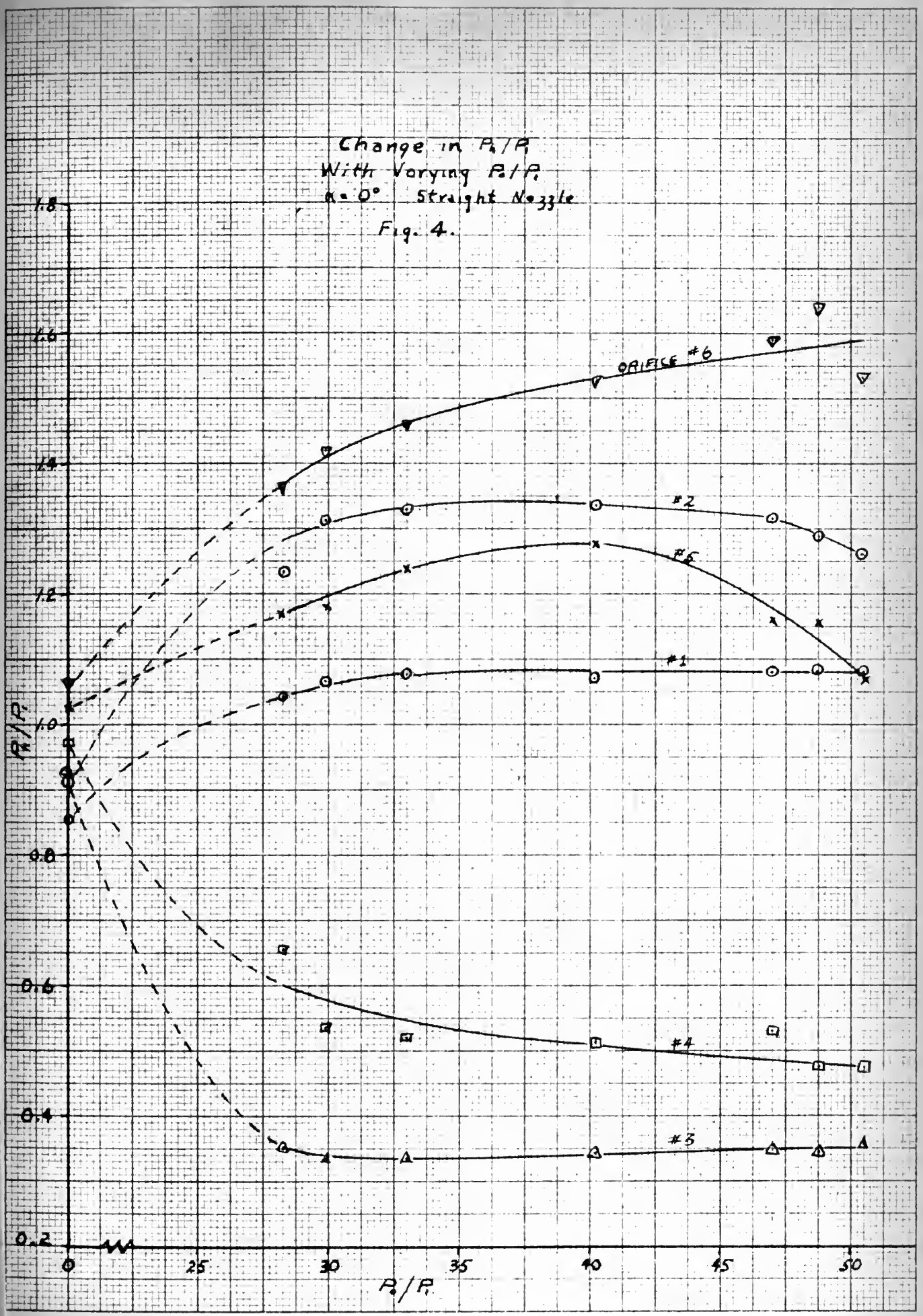

CHANGE IN P_h/P_1
WITH VARYING P_o/P_1
$\alpha = 0°$ STRAIGHT NOZZLE

FIG. 5.

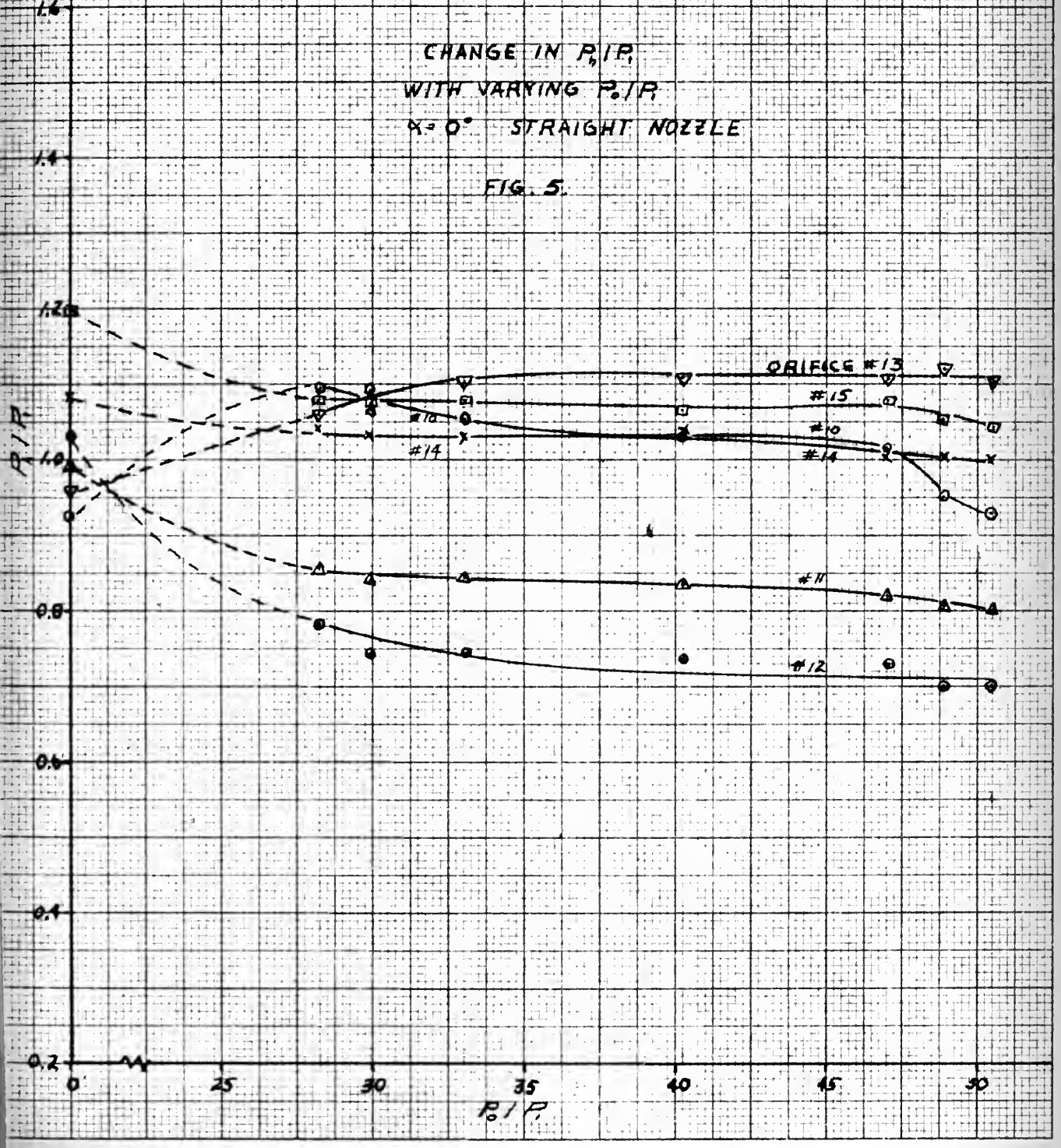

CHANGE IN P_2/P_1
WITH VARYING P_3/P_1
α-0° STRAIGHT NOZZLE

FIG. 6.

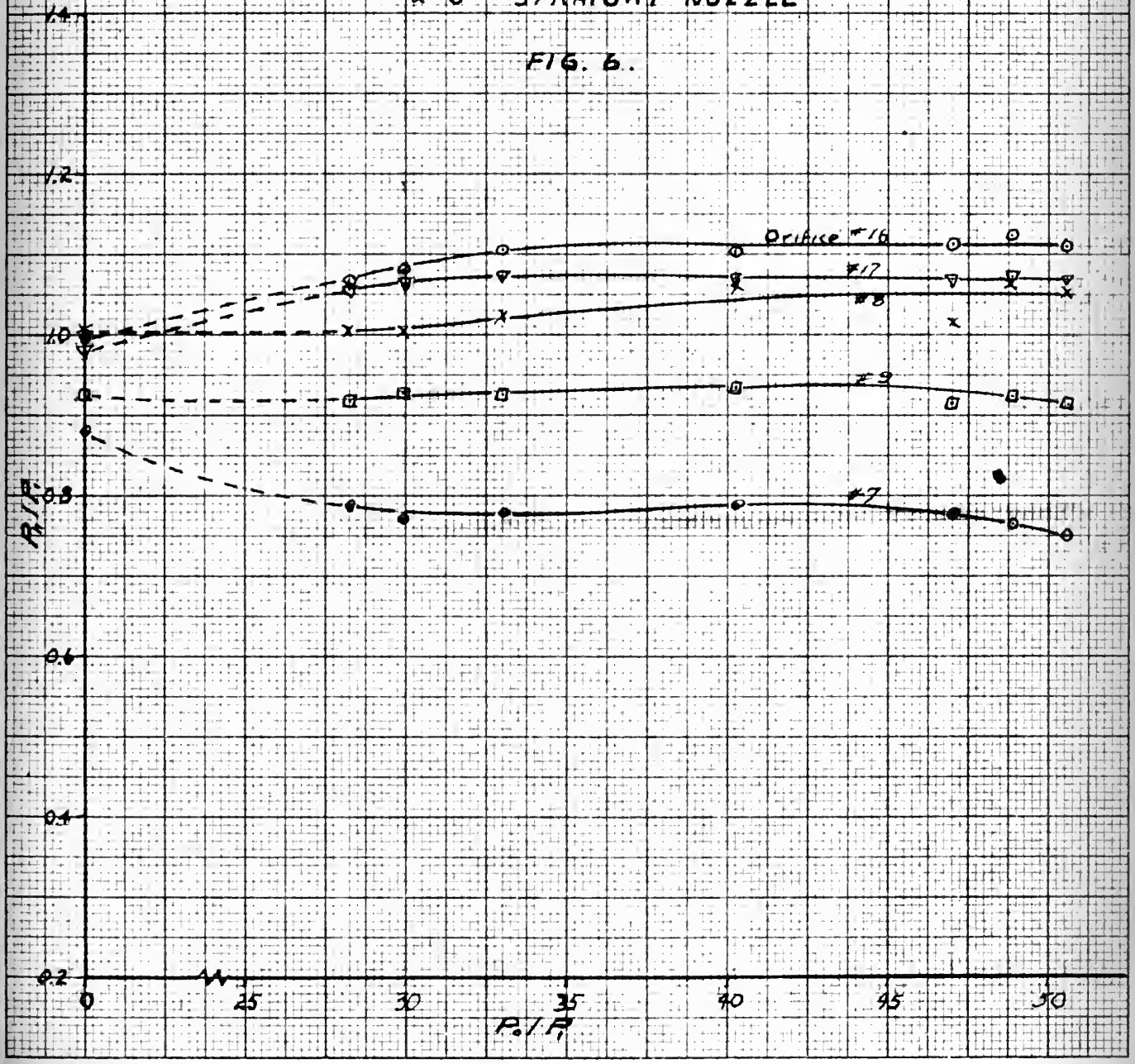

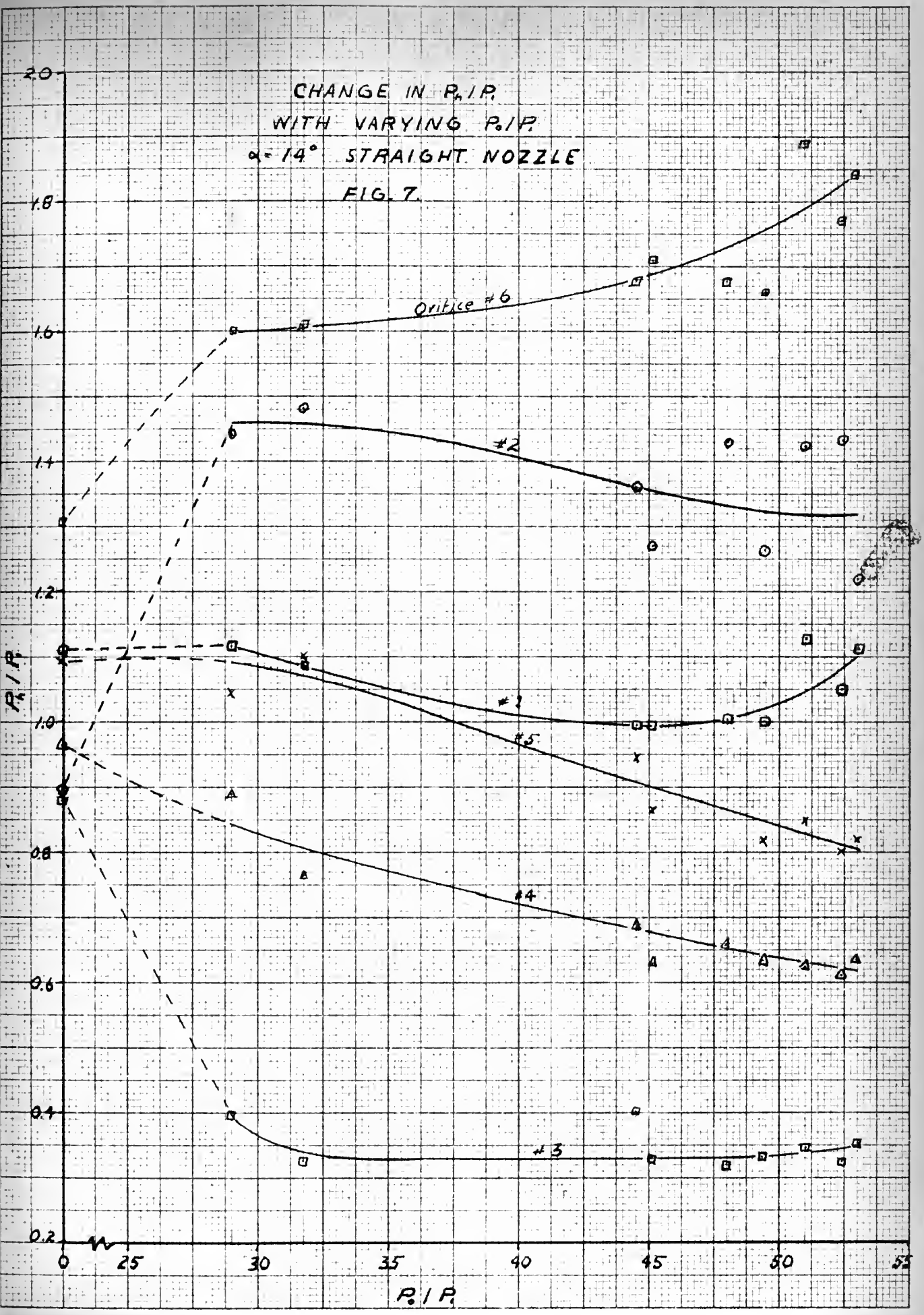
CHANGE IN P₂/P₁
WITH VARYING P₀/P₁
α = 14° STRAIGHT NOZZLE
FIG. 7
Orifice #6
#2
#1
#5
#4
#3
P₂/P₁
P₀/P₁
2.0
1.8
1.6
1.4
1.2
1.0
0.8
0.6
0.4
0.2
0
25
30
35
40
45
50
55

CHANGE IN P_4/P_1
WITH VARYING P_0/P_1
$\alpha = 14°$ STRAIGHT NOZZLE

FIG. 8.

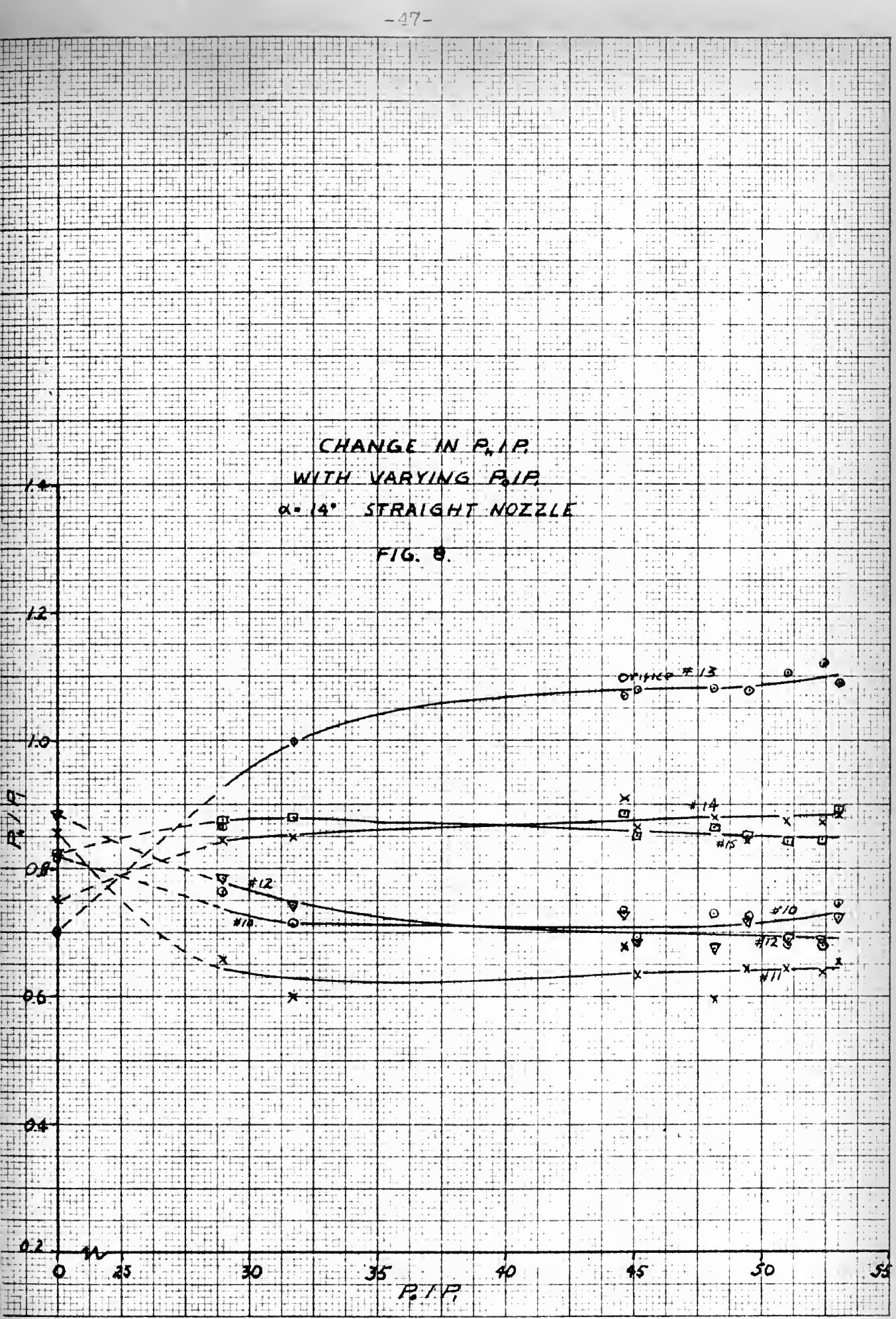

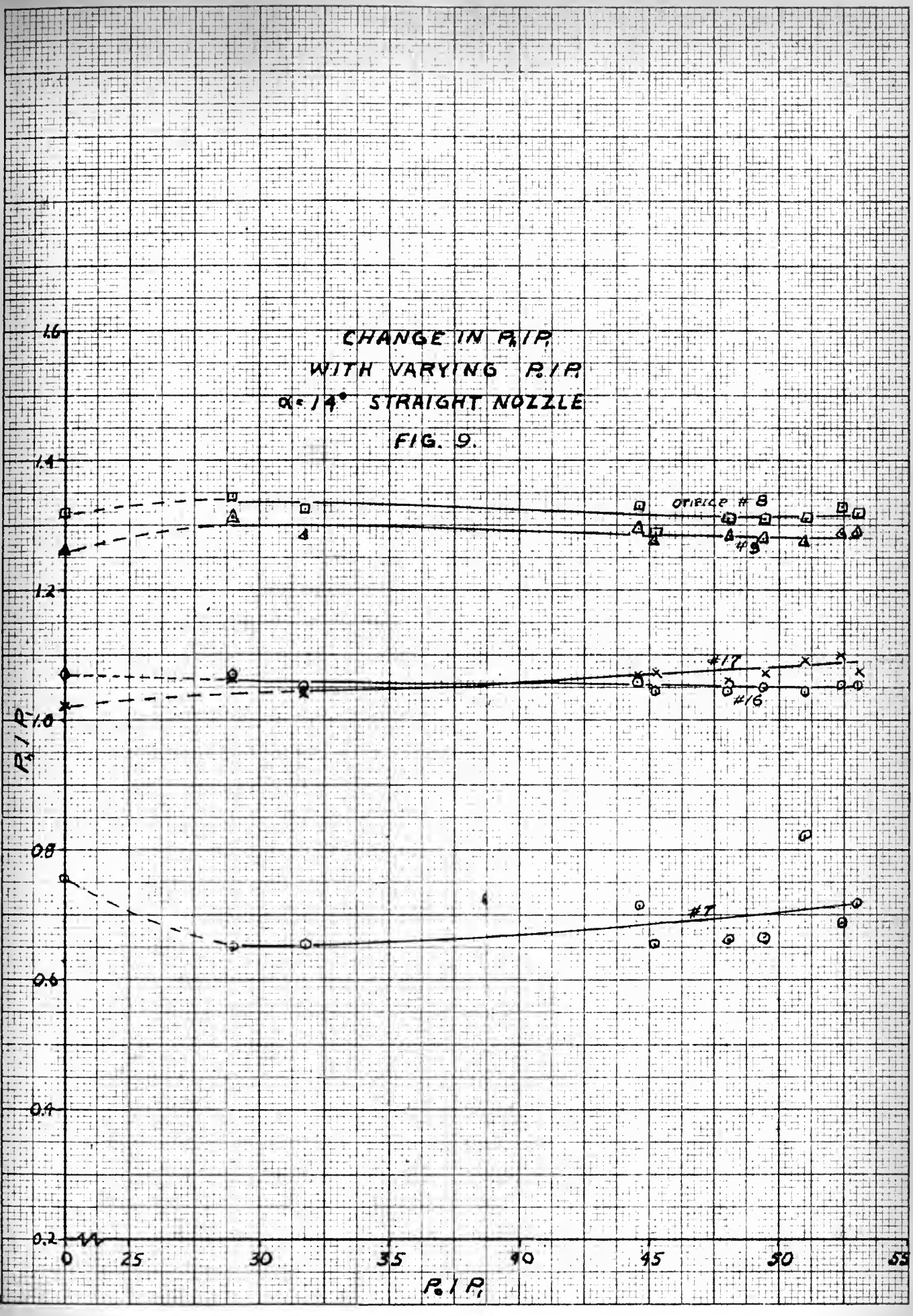
CHANGE IN P₂/P₁
WITH VARYING P₀/P₁
α = 14° STRAIGHT NOZZLE
FIG. 9.
ORIFICE # 8
#9
#17
#16
#7
P₂/P₁
P₀/P₁
1.6
1.4
1.2
1.0
0.8
0.6
0.4
0.2
0
25
30
35
40
45
50
55

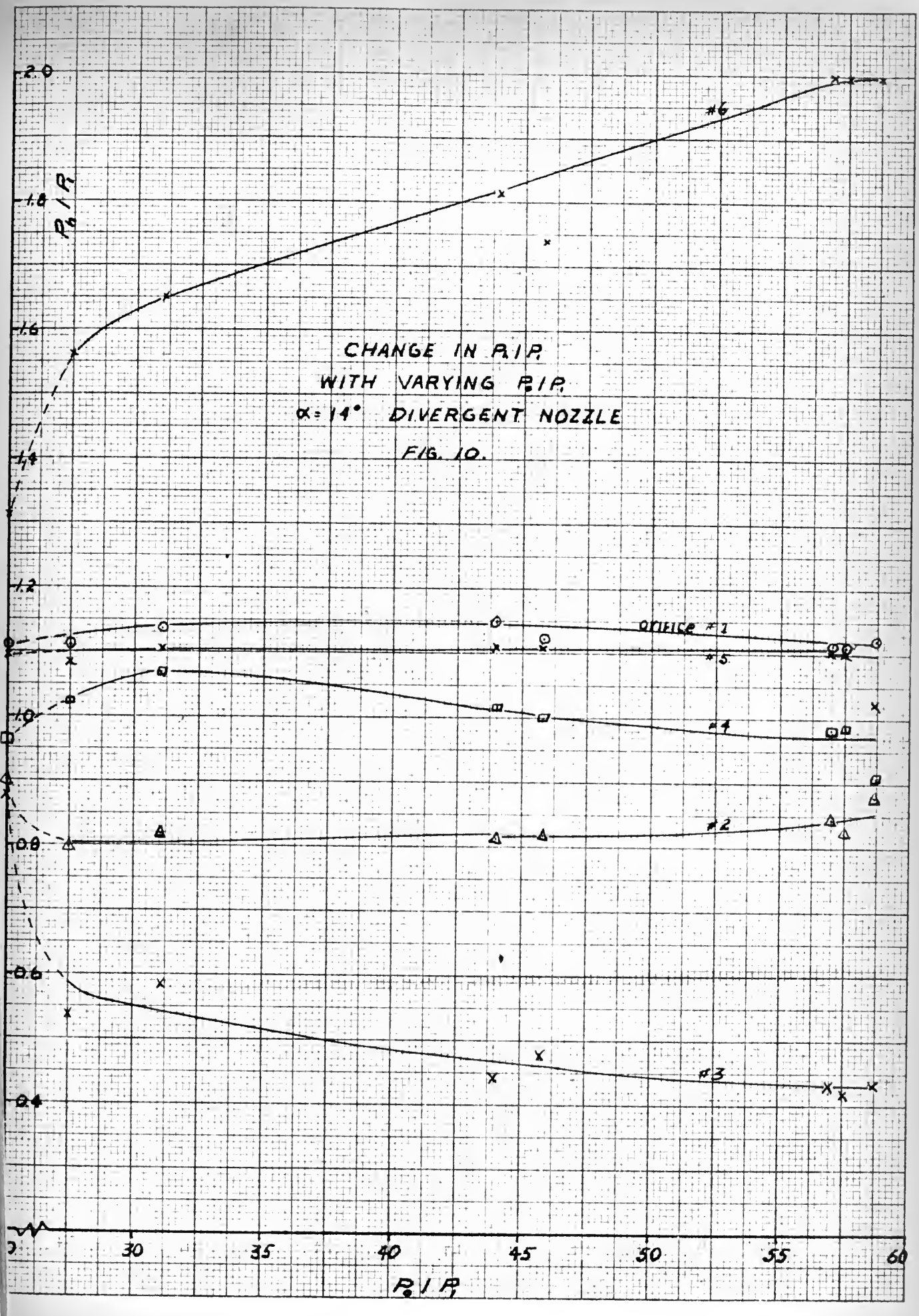

CHANGE IN P_2/P_1
WITH VARYING P_2/P_1
$\alpha = 14°$ DIVERGENT NOZZLE

FIG. 10.

CHANGE IN P_4/P_1
WITH VARYING P_0/P_1
$\alpha = 14°$ DIVERGENT NOZZLE
FIG. 11.

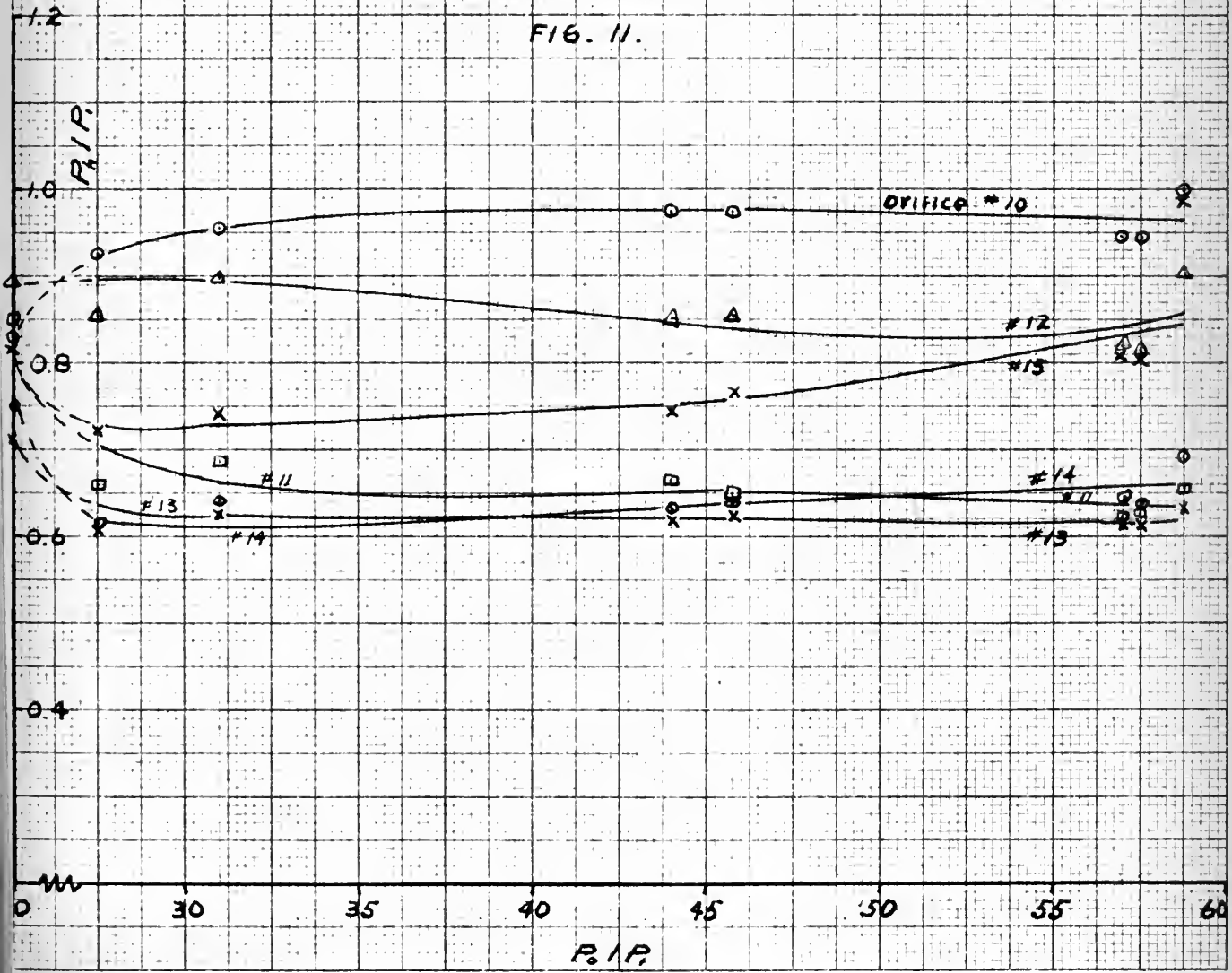

CHANGE IN P_2/P_1
WITH VARYING P_0/P_1
$\alpha = 14°$ DIVERGENT NOZZLE
FIG. 12.

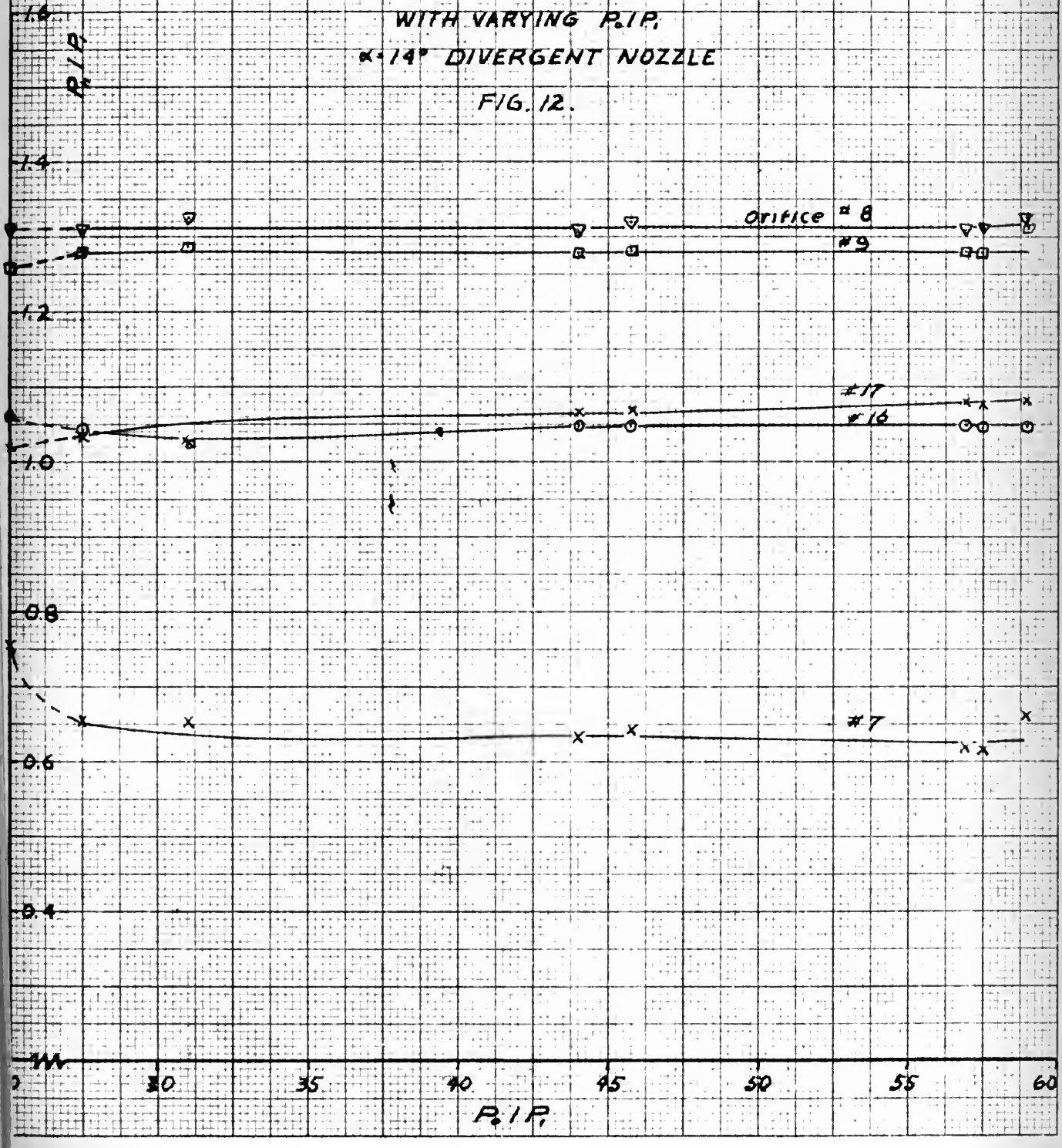

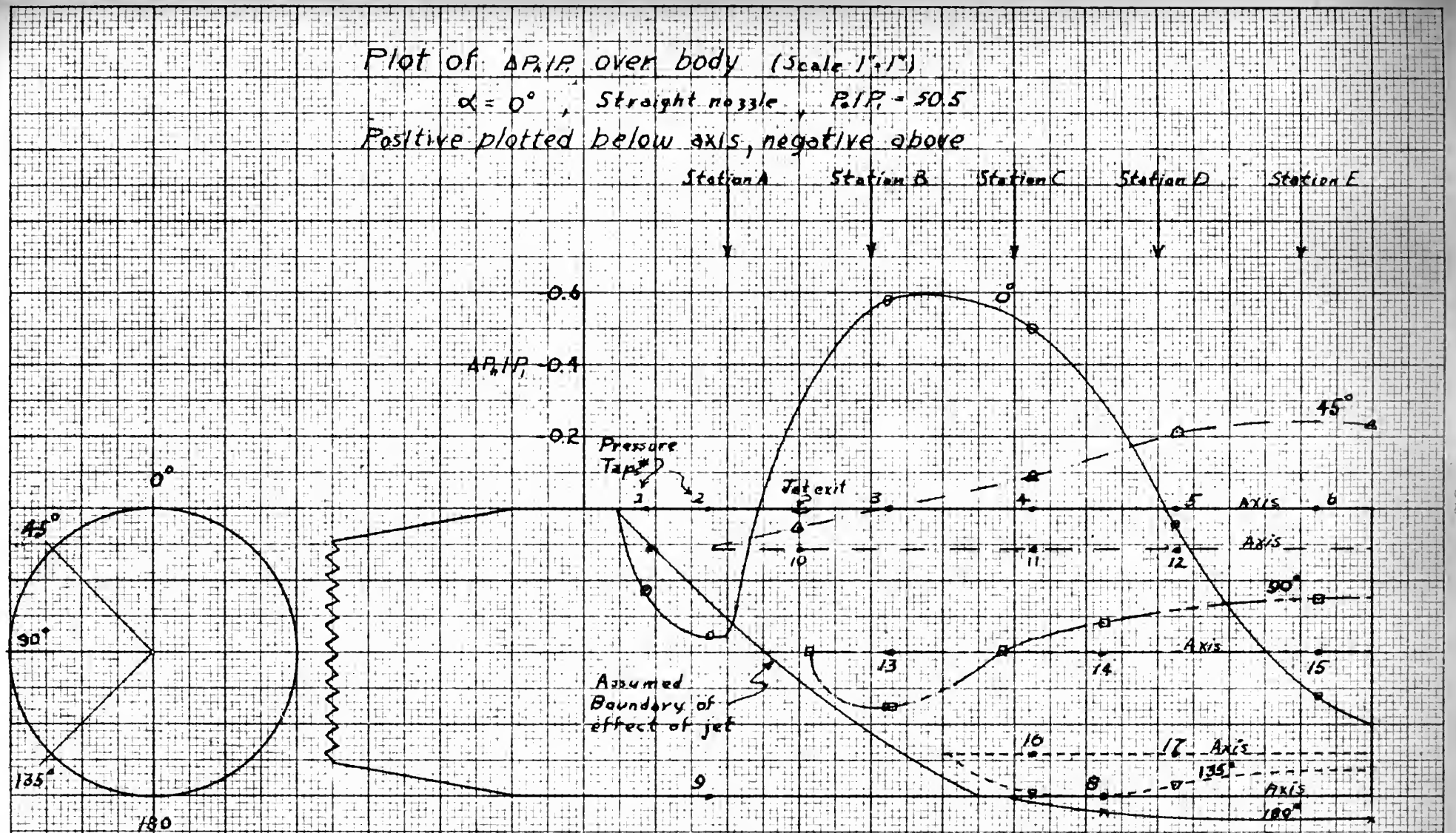
Plot of ΔP/P over body (Scale 1"=1")
α = 0°, Straight nozzle, P₀/P₁ = 50.5
Positive plotted below axis, negative above
Station A
Station B
Station C
Station D
Station E
0.6
ΔP/P 0.4
0.2
Pressure Taps
Jet exit
Axis
45°
90°
135°
180°
0°
Assumed Boundary of effect of jet
1
2
3
4
5
6
7
8
9
10
11
12
13
14
15
16
17

FIG. 13.

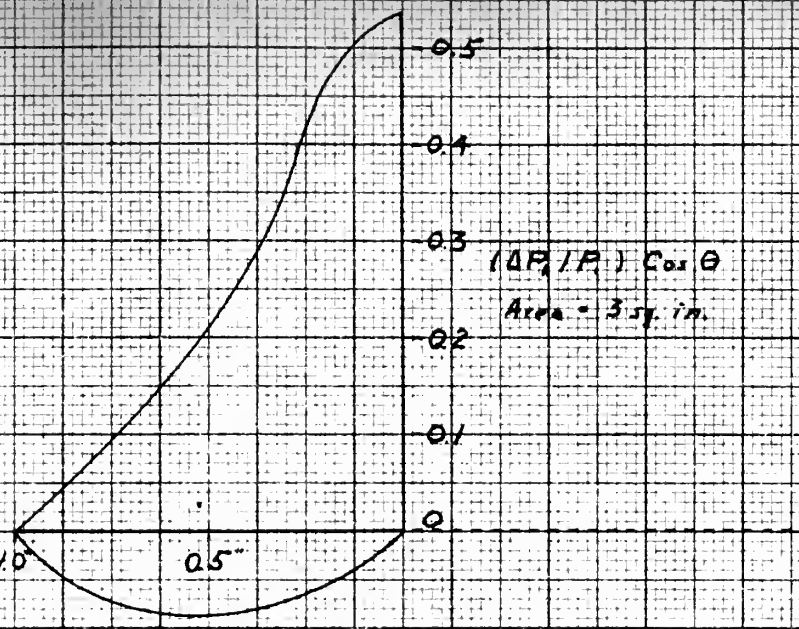

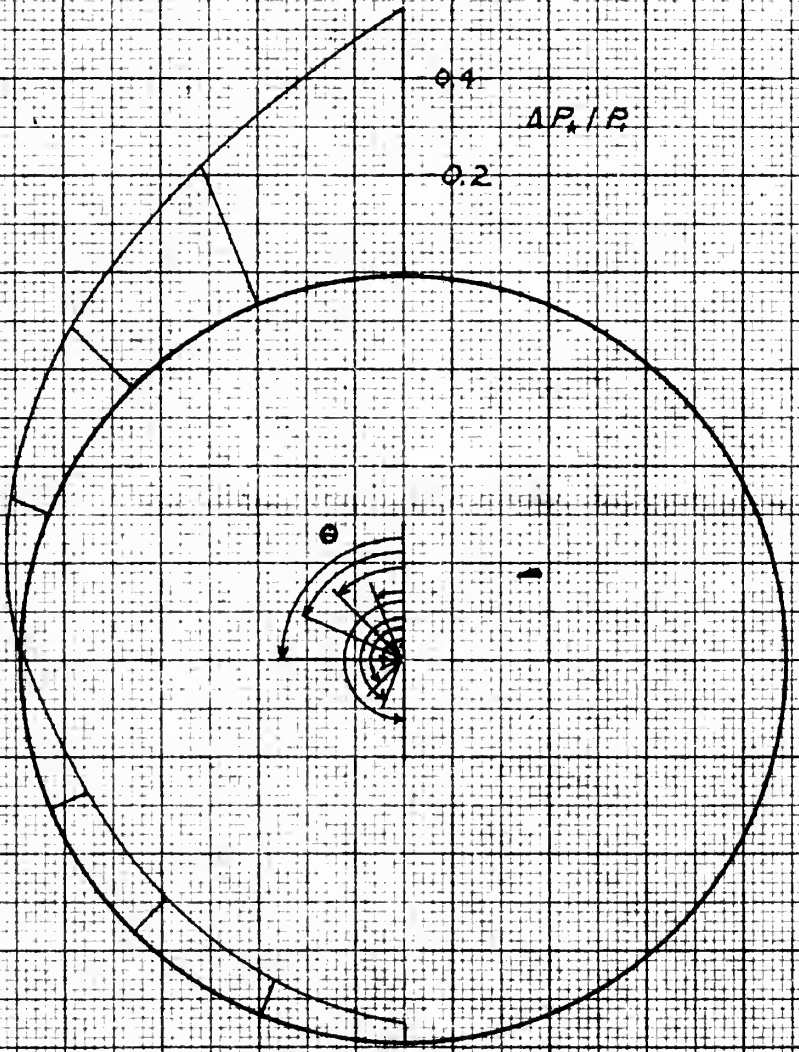

Integration of $\Delta P_x/P_t$ Station C

$\alpha = 0°$, Straight nozzle. $P_o/P_t = 50.5$

FIG. 14.

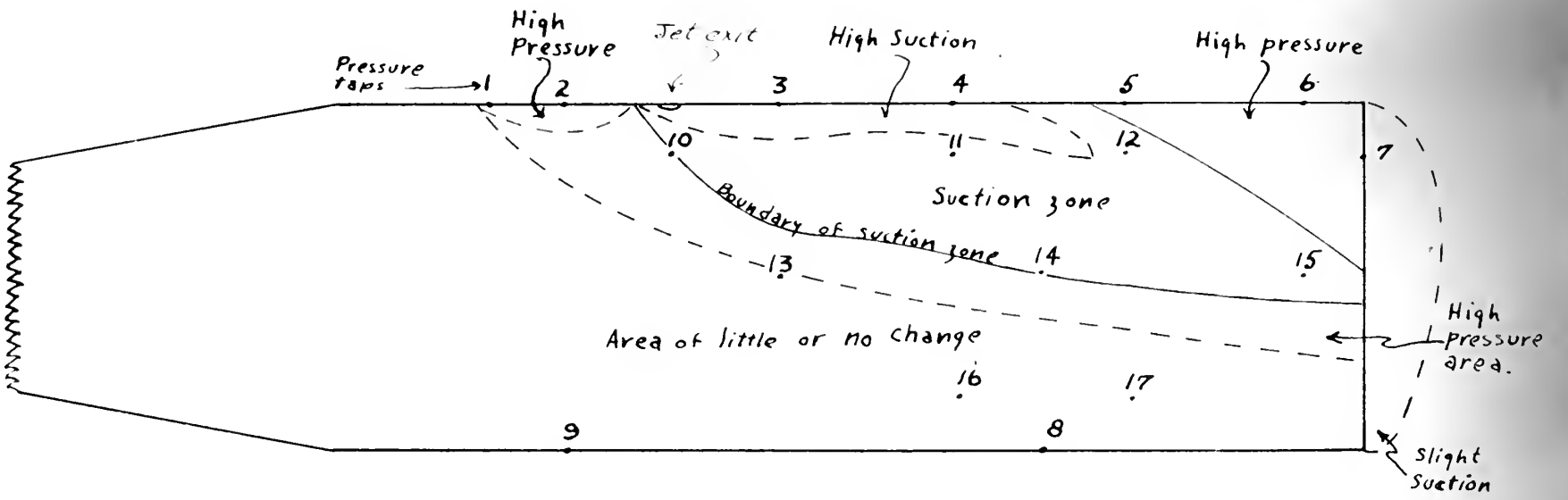

Approximate high pressure and low pressure (suction) zones due to jet. See Figs. 4, 5, and 6.

$\alpha = 0°$, straight nozzle. $P_0/P_1 = 50.5$

FIG. 15.

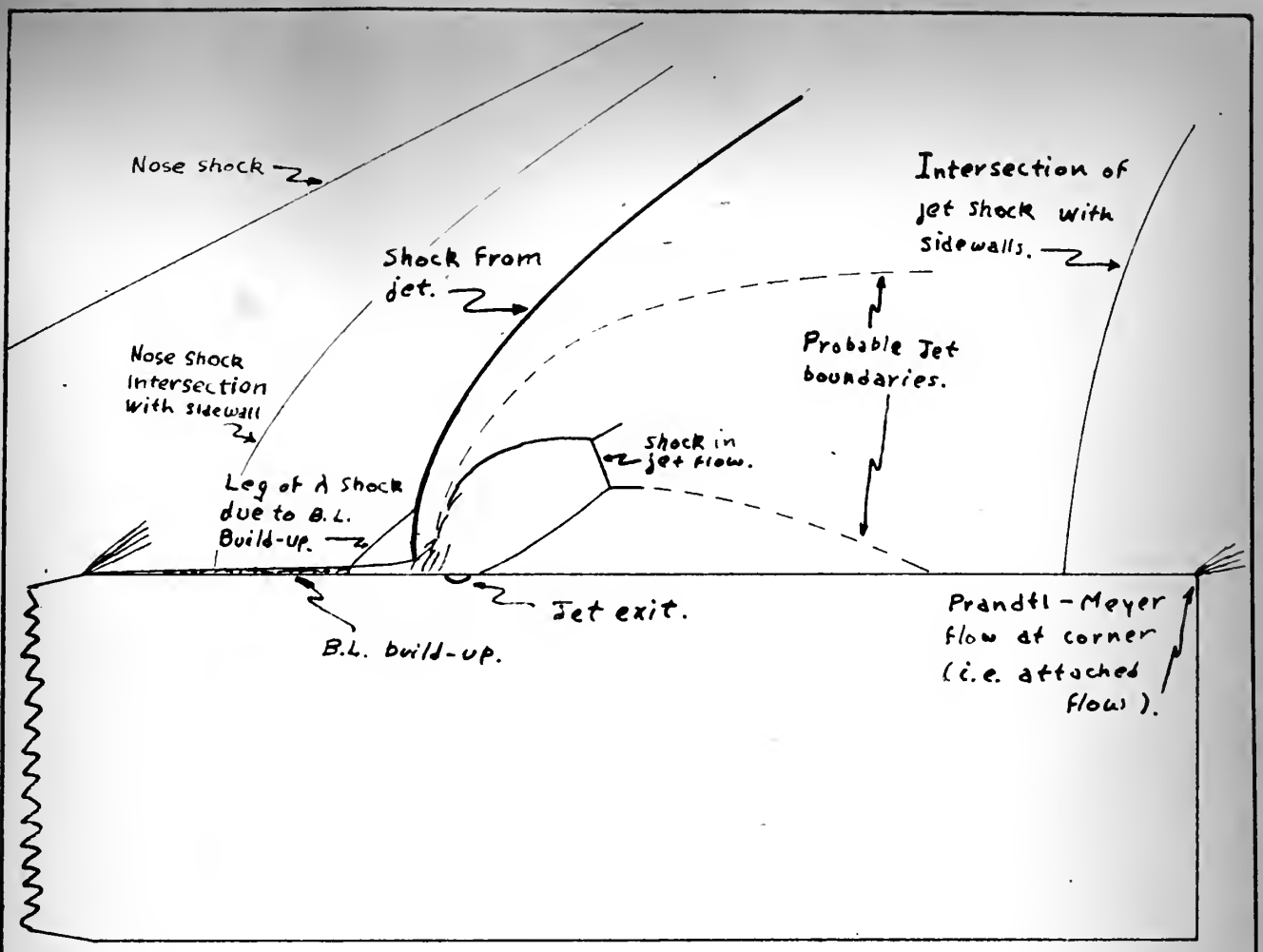

GENERAL SHOCK CONFIGURATION
($\alpha = 0°$)

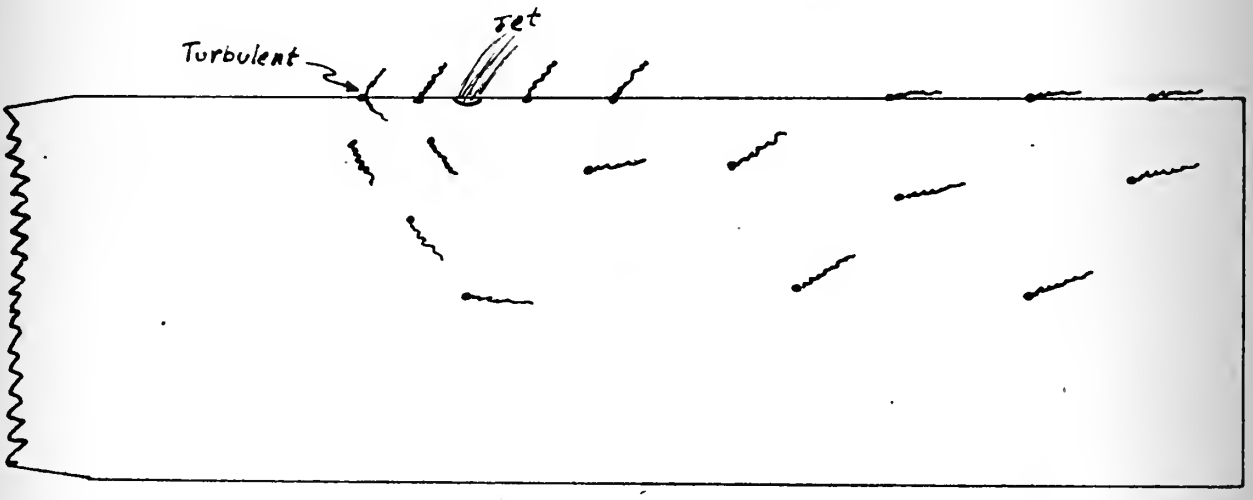

GENERAL FLOW PATTERN AS SHOWN BY TUFTS.

FIG. 15a.

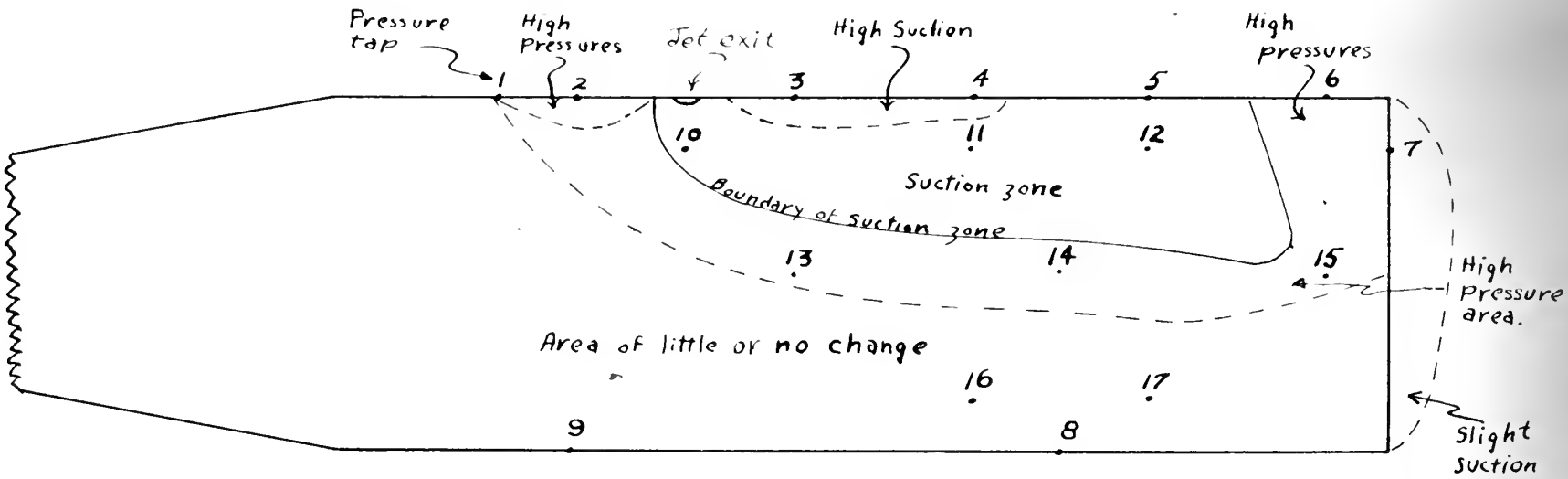

Approximate high pressure and low pressure (Suction) zones due to jet. See Figs 7, 8, and 9

$\alpha = 14°$, Straight nozzle., $P_o/P_1 = 53.0$

FIG. 16.

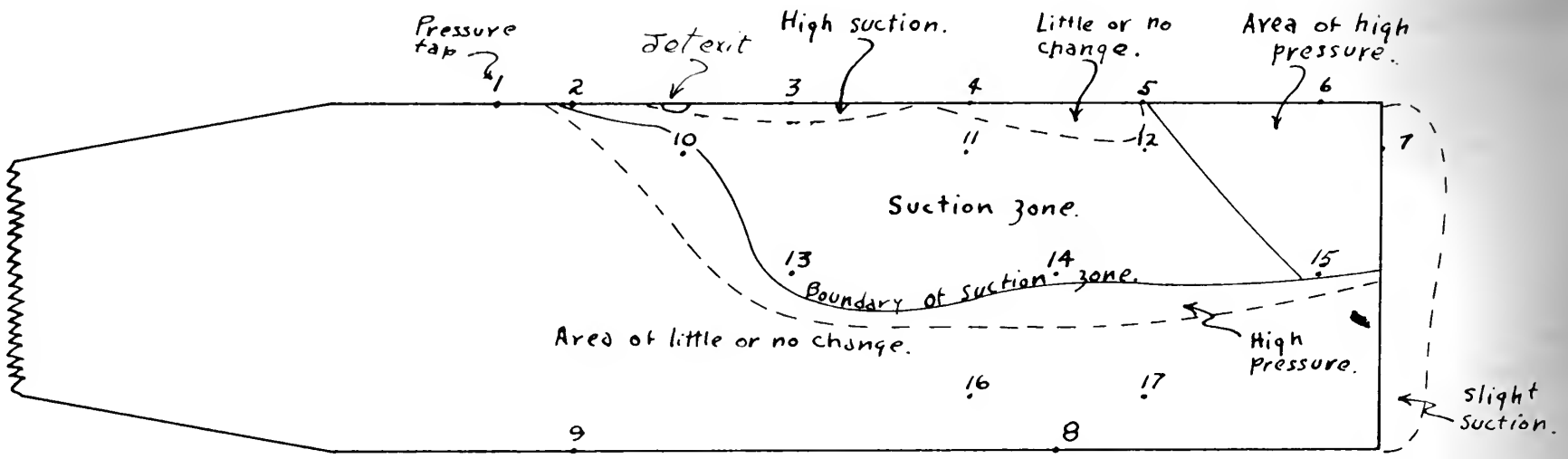

Approximate high and low pressure (suction) zones due to jet. See Figs. 10, 11, and 12.

$\alpha = 14°$ Divergent nozzle, $P_o/P_i = 58.7$.

FIG. 17.

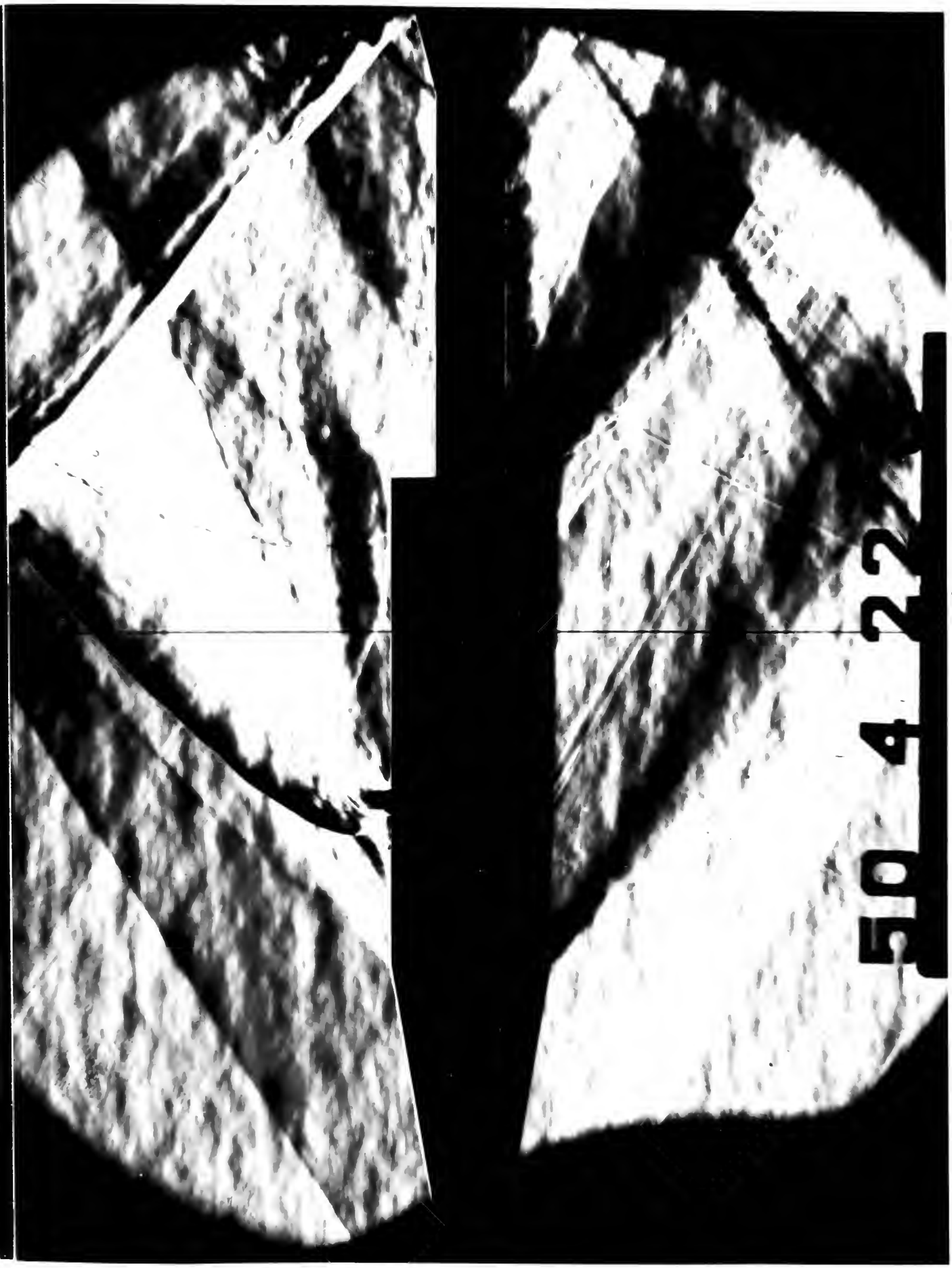

FIG. 18

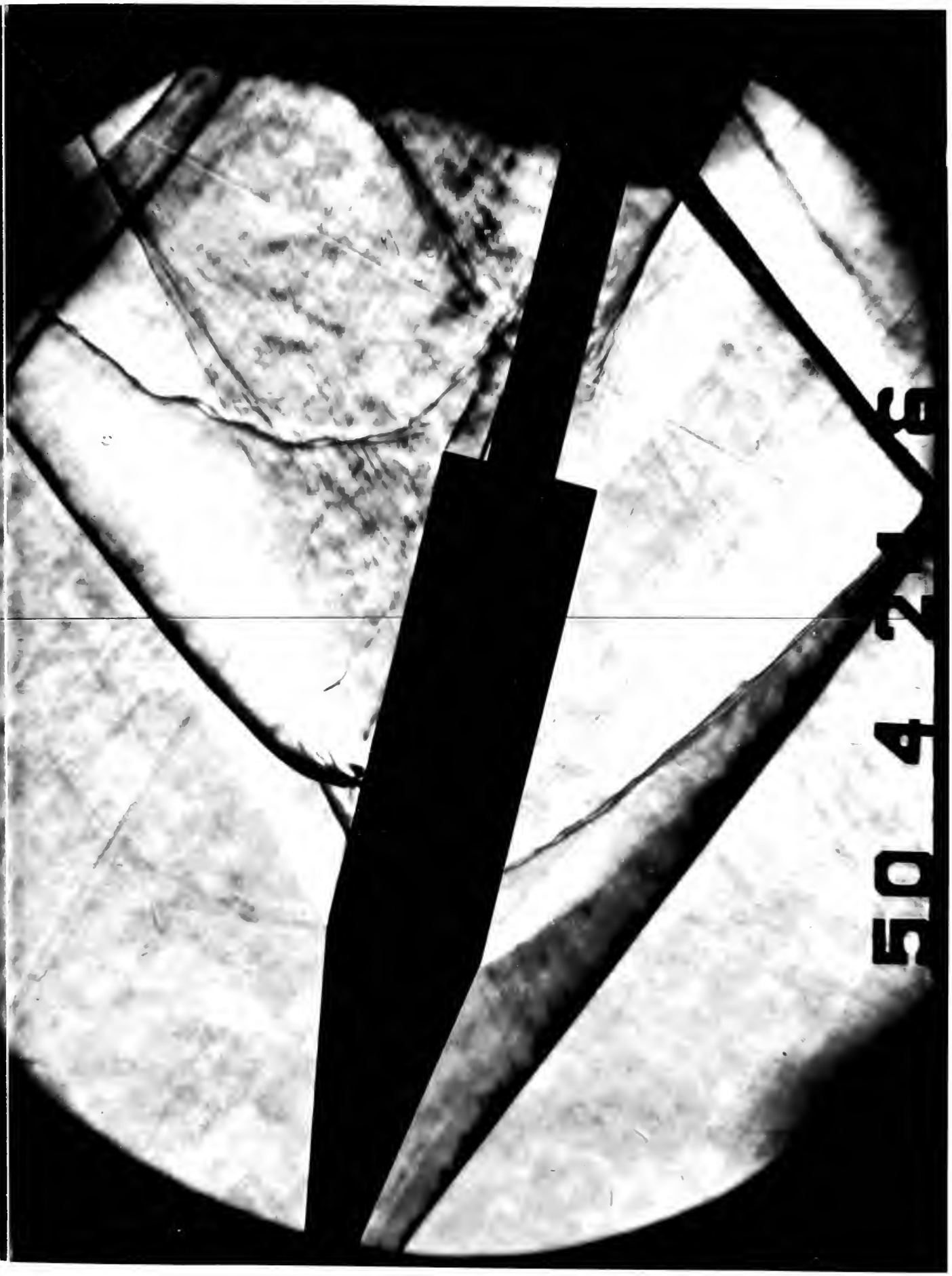

FIG. 19

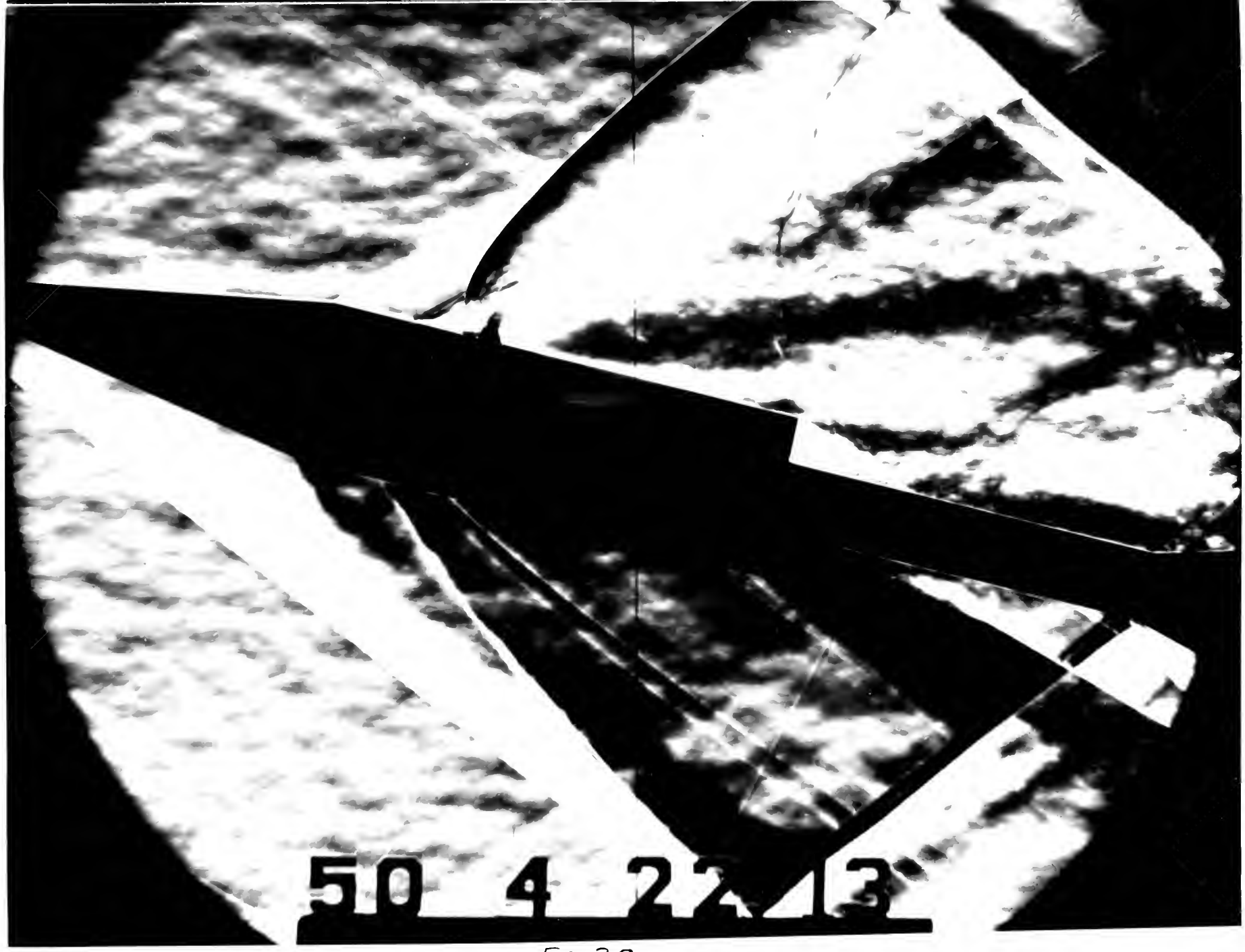

FIG. 20.

FIG. 21.

FIG. 22

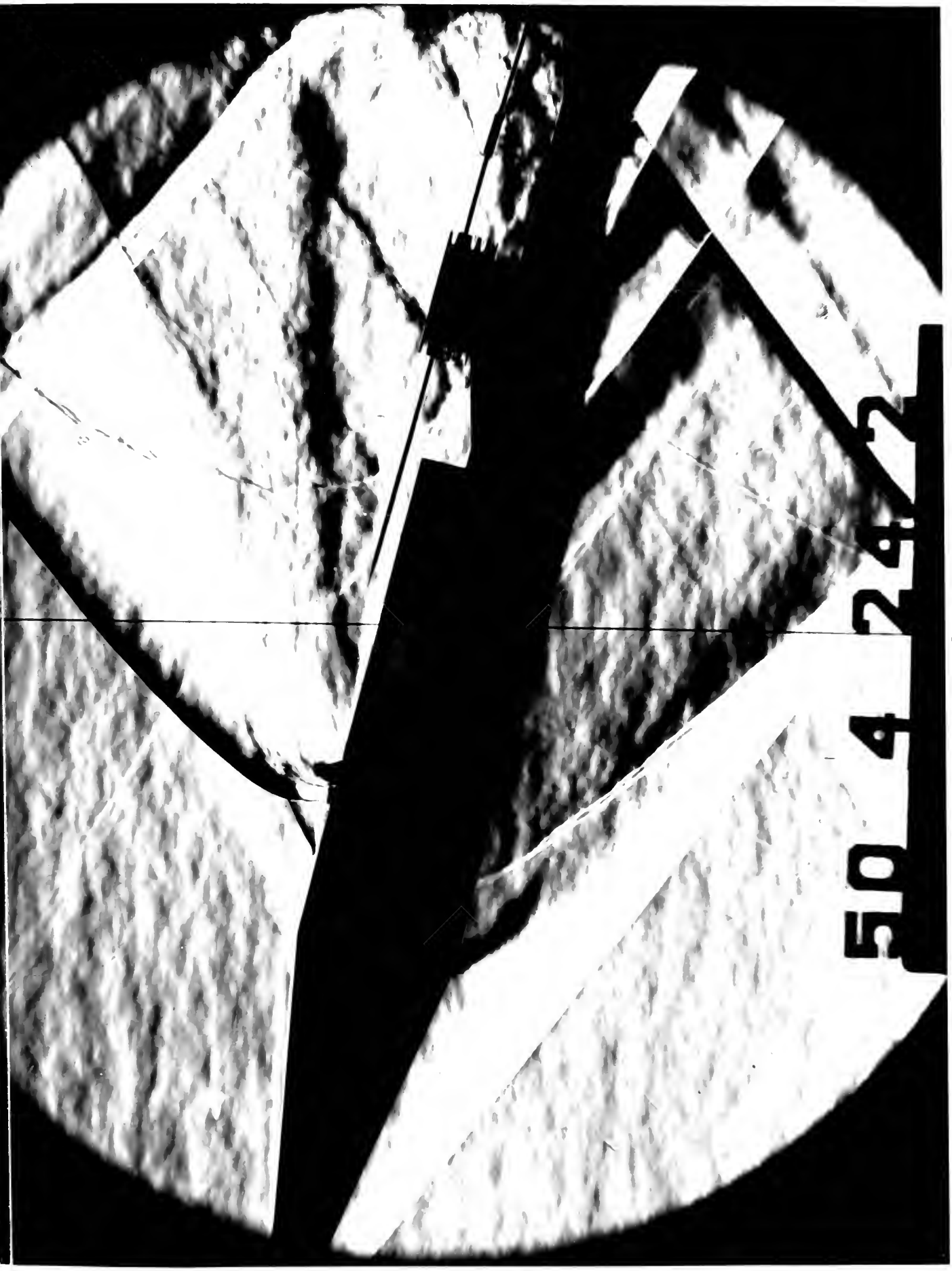

FIG. 23.

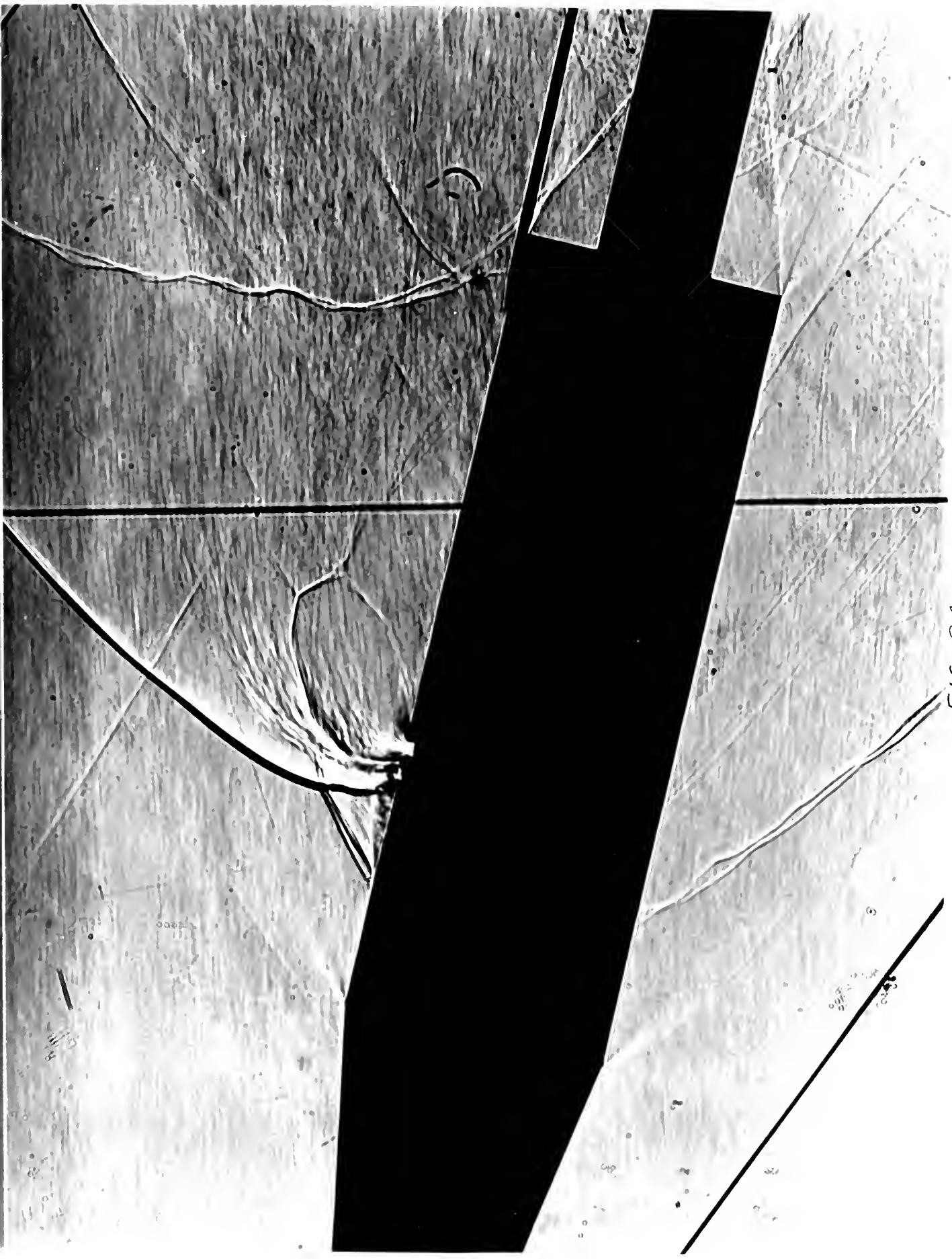

FIG. 24

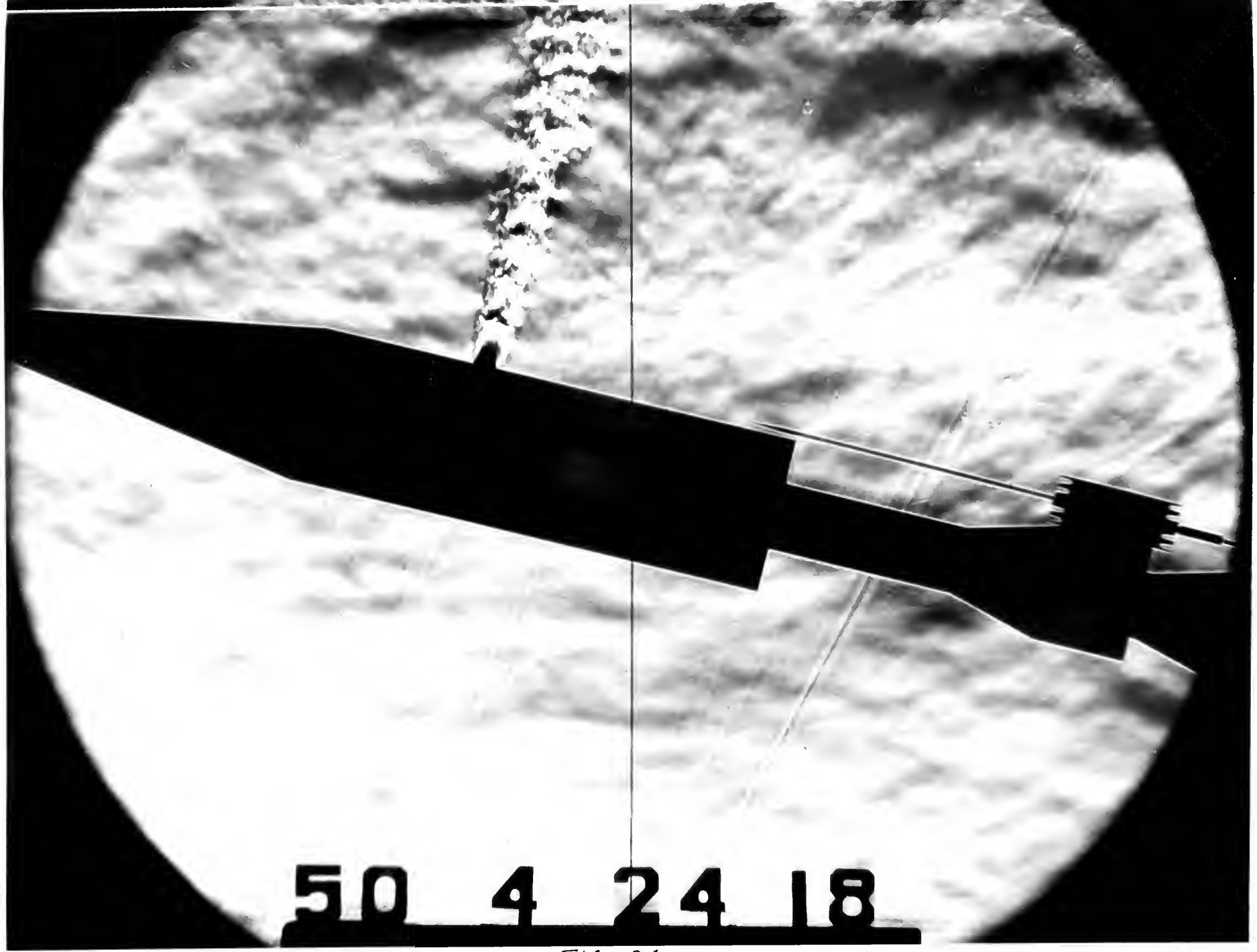

FIG. 24a

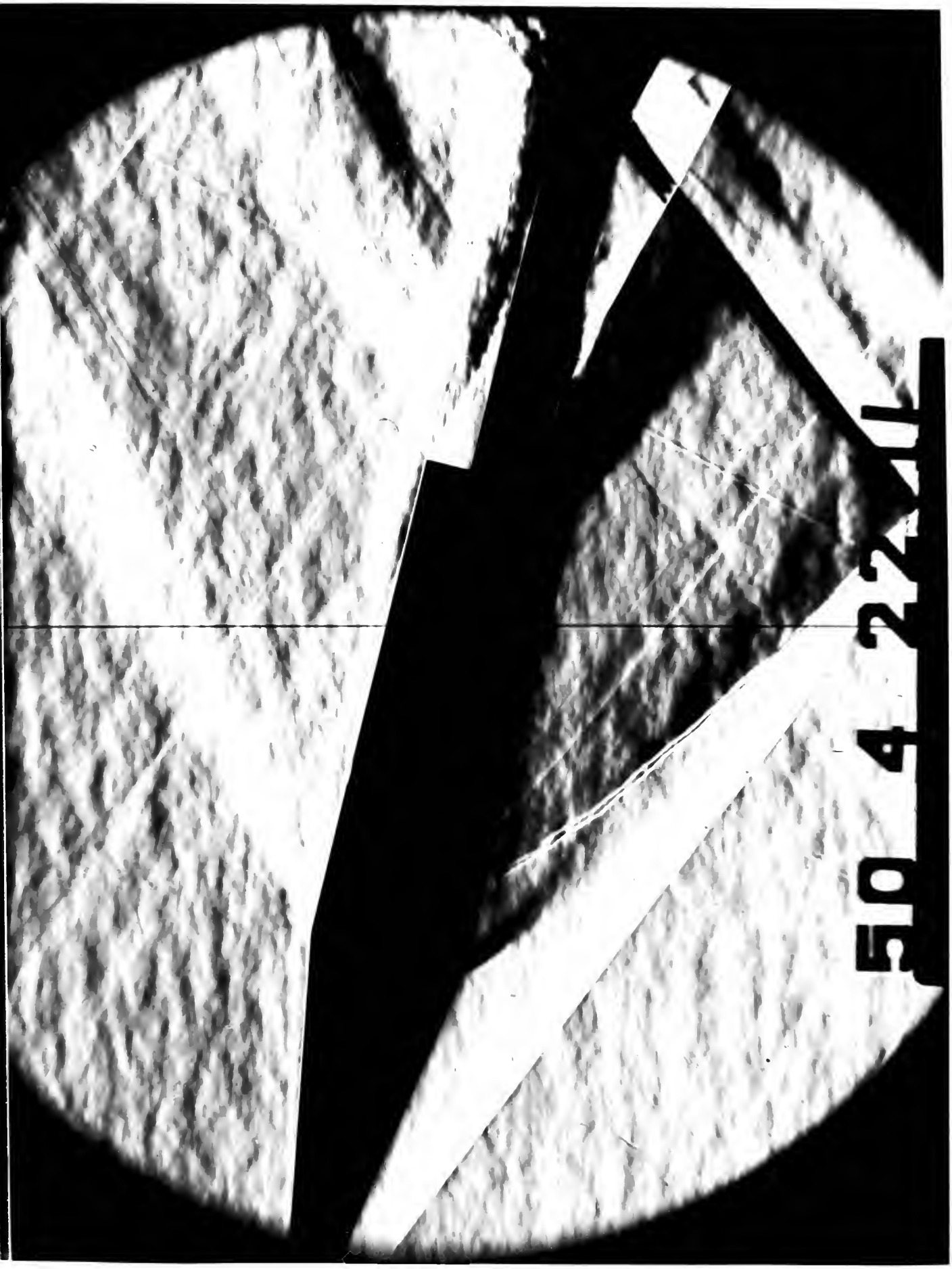

FIG. 25

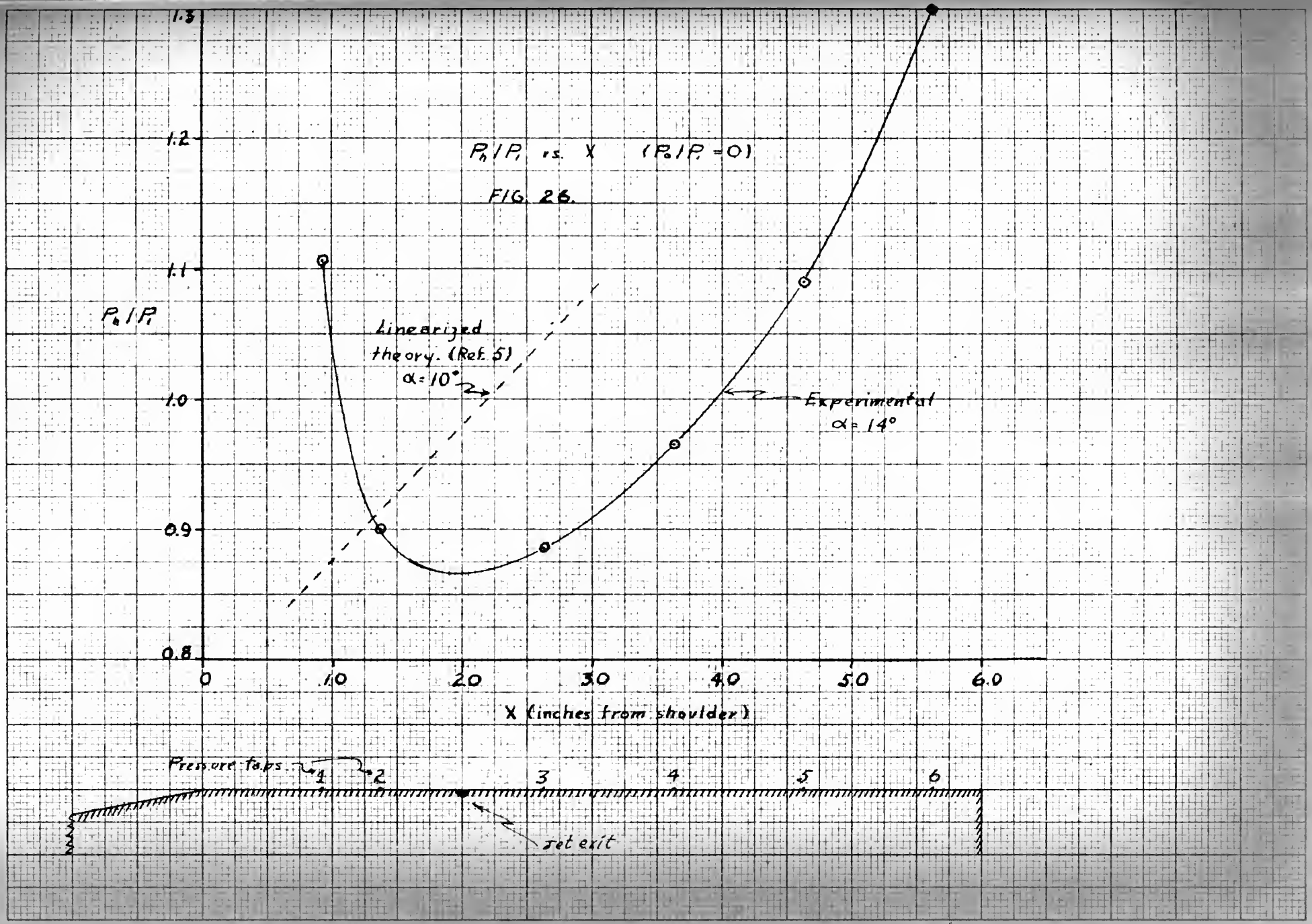
P_b/P_i vs. X ($P_o/P_i = 0$)
FIG. 26.
P_b/P_i
1.3
1.2
1.1
1.0
0.9
0.8
Linearized theory. (Ref. 5) $\alpha = 10°$
Experimental $\alpha = 14°$
0
1.0
2.0
3.0
4.0
5.0
6.0
X (inches from shoulder)
Pressure taps
1
2
3
4
5
6
Jet exit

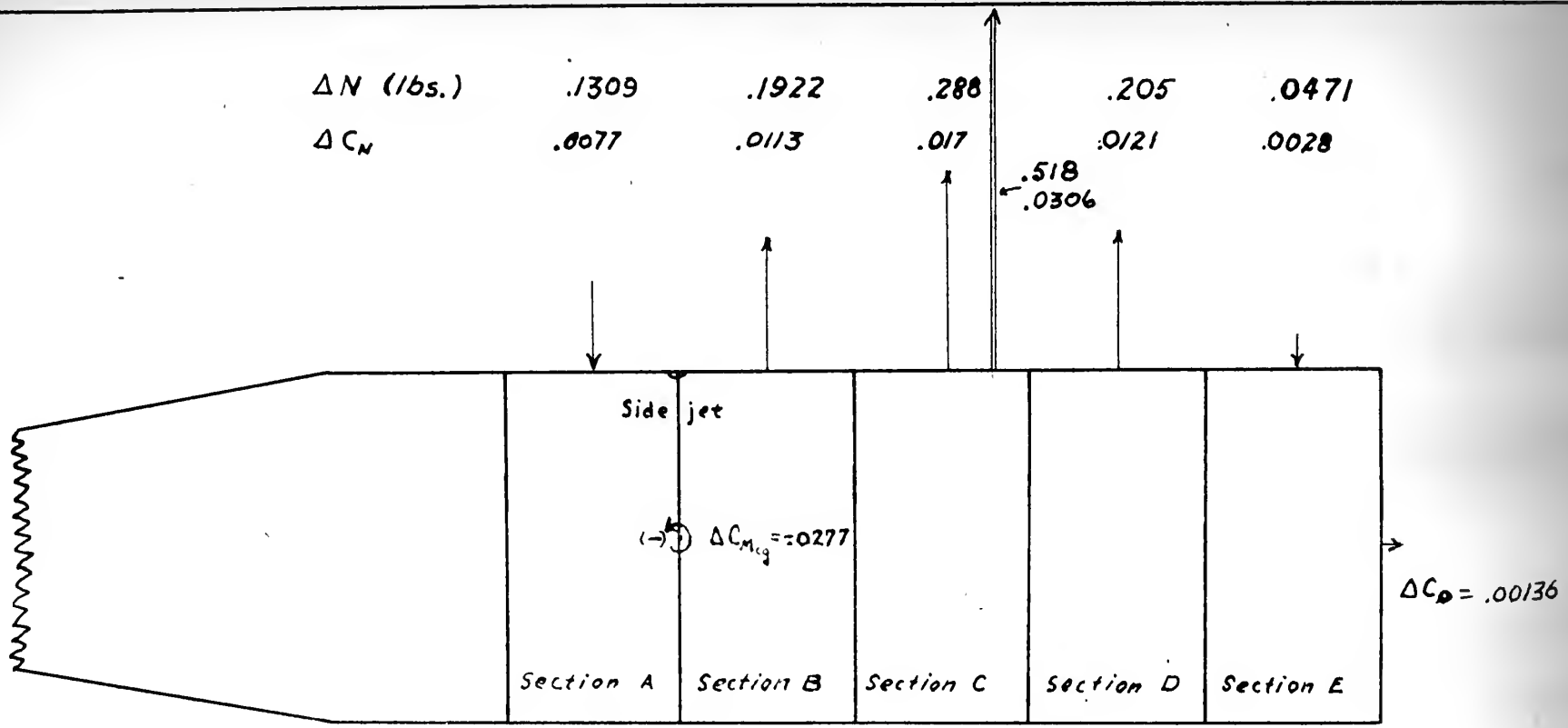

Change of
normal force and normal force coefficient
over the sections integrated (for maximum P_o/P_i)
$\alpha = 0°$ straight nozzle. Scale 1" = 1".

FIG. 27.

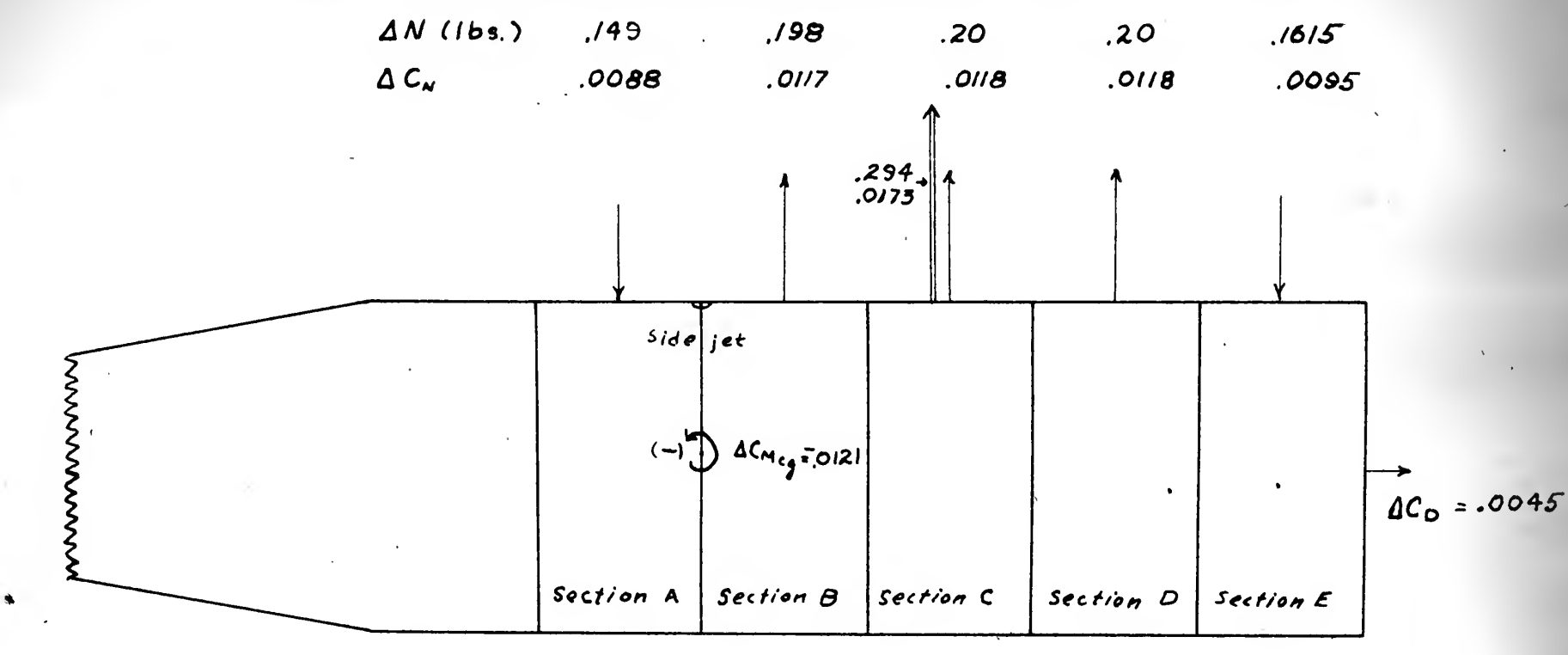

Change of
normal force and normal force coefficient
over the sections integrated (for maximum F_B/P_i)
α = 14° Straight Nozzle., Scale 1" = 1".

FIG. 28.

ΔN (lbs.)	.0265	.137	.087	.050	.1922
ΔC_N	.0016	.0081	.0051	.0029	.0113

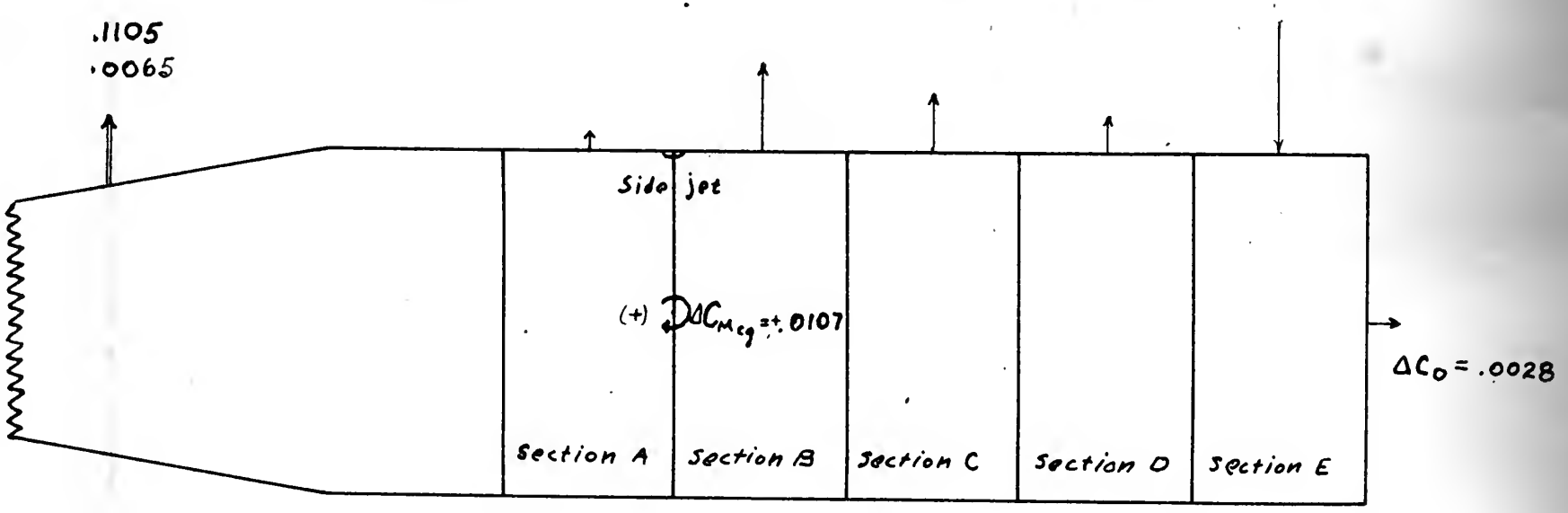

Change of
normal force and normal force coefficient
over the sections integrated (for maximum P_o/P_i).
$\theta = 14°$ Divergent nozzle., Scale 1" = 1".

FIG. 29.

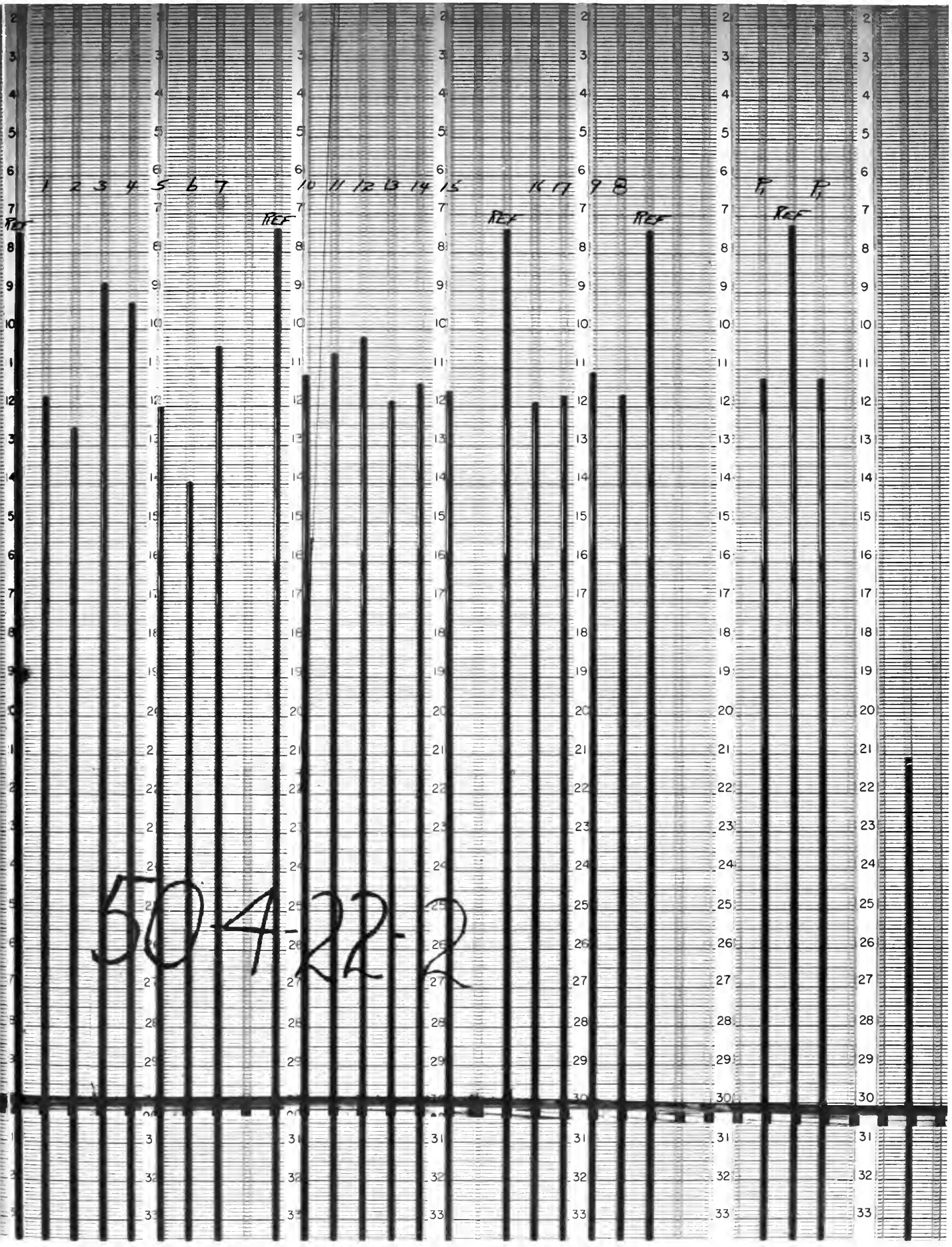

FIG. 29a

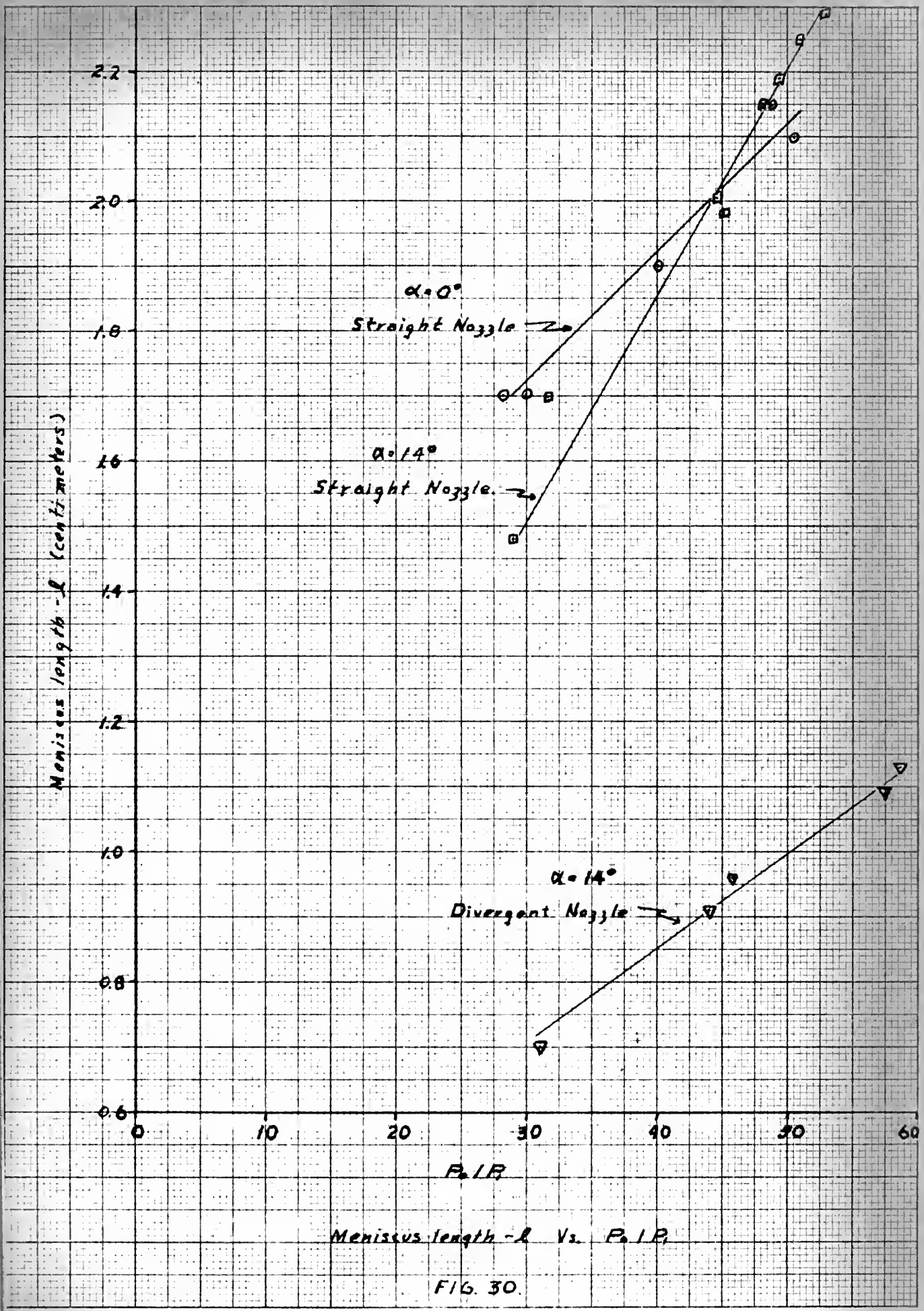

Meniscus length - ℓ Vs. P_0/P_1

FIG. 30.

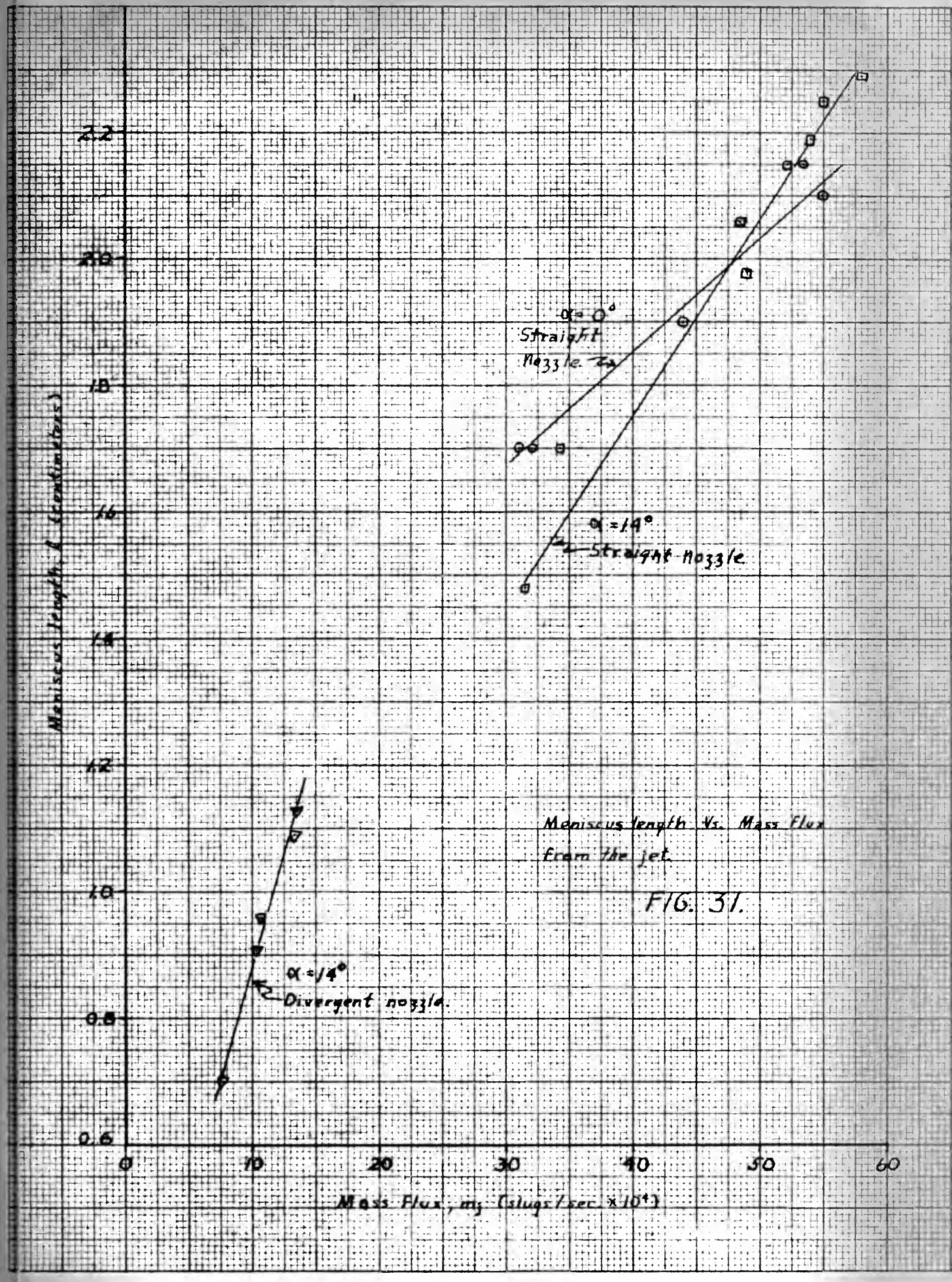

Meniscus length Vs. Mass flux from the jet.

FIG. 31.

					$\alpha = 0°$ STRAIGHT NOZZLE													
		TAP #1	#2	#3	#4	#5	#6	#7	#10	#11	#12	#13	#14	#15	#16	#17	#9	#8
RUN NO	P_3/P_1	P_1/P_1	P_1/P_1	P_1/P_1	P_4/P_1	P_5/P_1	P_6/P_1	P_7/P_1	P_{10}/P_1	P_{11}/P_1	P_{12}/P_1	P_{13}/P_1	P_{14}/P_1	P_{15}/P_1	P_{16}/P_1	P_{17}/P_1	P_9/P_1	P_8/P_1
4-21-1	0	.851	.900	.905	.945	1.000	1.026	.863	.920	.962	1.000	.933	1.075	1.15	.980	.960	.900	.977
4-21-2	0	.865	.935	.945	.995	1.050	1.083	.909	.958	1.017	1.059	.900	1.080	1.230	1.112	1.010	.950	1.033
4-22-6	28.3	1.041	1.230	.365	.665	1.167	1.359	.794	1.095	.840	.789	1.06	1.040	1.080	1.065	1.058	920	1.009
4-22-4	29.9	1.069	1.309	.350	.546	1.180	1.140	.776	1.090	.845	.751	1.069	1.031	1.069	1.080	1.067	.932	1.007
4-22-3	33.05	1.078	1.329	.351	.532	1.239	1.455	.783	1.051	.847	.753	1.101	1.032	1.078	1.104	1.075	.930	1.021
4-22-8	40.2	1.071	1.320	.362	.523	1.272	1.514	.791	1.030	.840	.741	1.108	1.037	1.068	1.100	1.071	.938	1.070
4-22-7	47.0	1.080	1.309	.362	.543	1.166	1.579	.784	1.048	.825	.736	1.104	1.013	1.080	1.110	1.070	.919	1.019
4-22-2	48.8	1.080	1.280	.358	.484	1.150	1.624	.767	.949	.809	.705	1.103	1.001	1.049	1.120	1.086	.925	1.063
4-21-3	50.5	1.080	1.250	.354	.485	1.091	1.527	.755	.929	.805	.705	1.100	.999	1.041	1.100	1.067	.919	1.054
					$\alpha = 14°$ STRAIGHT NOZZLE													
4-22-10	0	1.110	.935	.854	.950	1.110	1.327	.779	.861	.871	.883	.762	.789	.854	1.080	1.023	1.262	1.309
4-22-11	0	1.113	.866	.915	.980	1.077	1.292	.740	.800	.844	.894	.678	.725	.602	1.047	1.017	1.280	1.317
4-24-4	28.95	1.114	1.430	.411	.892	1.044	1.590	.683	.768	.665	.790	.965	.847	.880	1.070	1.070	1.309	1.340
4-24-6	31.70	1.090	1.470	.342	.773	1.102	1.598	.665	.720	.608	.747	1.000	.852	.883	1.050	1.046	1.282	1.320
4-22-13	44.6	.895	1.352	.414	.693	.948	1.660	.720	.741	.686	.734	1.064	.810	.888	1.058	1.063	1.290	1.325
4-22-14	45.1	.995	1.265	.344	.638	.865	1.698	.661	.698	.641	.694	1.081	.868	.865	1.045	1.073	1.271	1.284
4-22-16	48.1	1.067	1.430	.336	.668	.905	1.668	.670	.737	.605	.685	1.080	.885	.870	1.048	1.059	1.280	1.308
4-22-15	49.4	1.001	1.260	.346	.643	.825	1.644	.671	.725	.651	.720	1.077	.851	.854	1.049	1.074	1.278	1.306
4-24-2	51.0	1.126	1.412	.361	.632	.854	1.871	.826	.690	.652	.690	1.105	.879	.846	1.047	1.088	1.270	1.310
4-24-3	52.4	1.050	1.422	.338	.619	.805	1.753	.695	.689	.647	.695	1.118	.879	.850	1.054	1.098	1.280	1.321
4-24-17	53.0	1.111	1.210	.364	.645	.823	1.820	.725	.754	.675	.731	1.089	.889	.894	1.054	1.071	1.285	1.311

P_4/P_1 AT EACH ORIFICE

TABLE I

$\alpha = 14^0$ DIVERGENT NOZZLE

RUN NO	P_0/P_1	Tap # 1 P_1/P_1	2 P_2/P_1	3 P_3/P_1	4 P_4/P_1	5 P_5/P_1	6 P_6/P_1	7 P_7/P_1	10 P_{10}/P_1	11 P_{11}/P_1	12 P_{12}/P_1	13 P_{13}/P_1	14 P_{14}/P_1	15 P_{15}/P_1	16 P_{16}/P_1	17 P_{17}/P_1	9 P_9/P_1	5 P_5/P_1
4-22-10	0	1.110	.935	.854	.950	1.110	1.327	.779	.861	.871	.883	.762	.789	.854	1.080	1.023	1.262	1.309
4-22-11	0	1.113	.866	.915	.980	1.177	1.292	.740	.800	.844	.894	.678	.725	.802	1.047	1.017	1.280	1.317
4-24-13	27.95	1.135	.804	.563	1.024	1.095	1.548	.623	.926	.668	.858	.616	616	.728	1.042	1.042	1.271	1.309
4-24-14	34.1	1.147	.825	.593	1.069	1.102	1.634	.664	.955	.695	.900	.638	.645	.750	1.024	1.021	1.281	1.320
4-24-11	44.0	1.122	.819	.454	1.020	1.099	1.80	.644	.976	.672	.851	.626	.642	.751	1.048	1.069	1.273	1.311
4-24-12	45.8	1.124	.825	.491	1.000	1.100	1.723	.651	.978	.656	.858	.631	.650	.775	1.050	1.070	1.280	1.312
4-24-8	56.9	1.105	.847	.442	.983	1.080	1.980	.628	.925	.630	.822	.634	.653	.817	1.050	1.080	1.278	1.308
4-24-9	57.5	1.105	.826	.430	.990	1.076	1.980	.624	.950	.636	.820	.620	.644	.811	1.047	1.076	1.275	1.308
4-24-15	58.7	1.120	.879	.484	.909	1.024	1.930	.667	1.002	.665	.907	.642	.699	1.028	1.048	1.080	1.311	1.317

P_i/P_1 AT EACH ORIFICE

TABLE I (CONT'D)

	$\alpha = 0°$ STRAIGHT NOZZLE										
SECTION		A	B	C	D	E	RESULTANT	ON BASE	MOM.	TOTAL	
AREA	SQ.IN.	-2.72	9.0	6.0	4.26	-.98	10.56				
NORMAL FORCE	LBS.	-.1309	.1922	.288	.205	-.0471	.518	.021			
C_N		-.0077	.013	.0170	.0121	-.0028	.0306				
DRAG	LBS.						0	.0231			
C_D							0	.00136		.00136	
$C_{M_{C.G.}}$									-.0277	-.0277	
C_L							.0306			.0306	
	$\alpha = 14°$ STRAIGHT NOZZLE										
AREA		-.31	4.12	4.16	4.16	-3.36	6.98				
NORMAL FORCE		-.149	.198	.20	.20	-.1615	.294	.0054			
C_N		-.0088	.0117	.0118	.0118	-.0095	.0173				
DRAG								.0052			
C_D							.0042	.00031		.0045	
$C_{M_{C.G.}}$									-.0121	-.0121	
C_L							.0162			.0162	
	$\alpha = 14°$ DIVERGENT NOZZLE										
AREA		.55	2.85	1.81	1.04	-4.0	2.25				
NORMAL FORCE		.0265	.137	.087	.050	-.1922	.1105	.0205			
C_N		.0016	.0081	.0051	.0029	-.0113	.0065				
DRAG								.0198			
C_D							.0016	.0017		.0028	
$C_{M_{C.G.}}$									.0107	.0107	
C_L							.0013				

RESULTS OF INTEGRATION OF PRESSURE DISTRIBUTION

TABLE II

$\alpha = 0°$ Straight Nozzle			$\alpha = 14°$ Straight Nozzle			$\alpha = 14°$ Divergent Nozzle		
Run No.	P_0/P_1	Meniscus Length Cm	Run No	P_0/P_1	Meniscus Length Cm.	Run No	P_0/P_1	Meniscus Length Cm
4-22-6	28.3	1.70	4-24-9	28.95	1.46	4-24-14	30.1	.70
4-22-4	29.9	1.70	4-24-6	31.7	1.70	4-24-11	44.0	.91
4-22-8	40.2	1.90	4-22-13	44.6	2.06	4-24-12	45.6	.96
4-22-2	48.8	2.15	4-22-14	45.1	1.98	4-24-9	57.5	1.09
4-21-3	50.5	2.10	4-22-16	45.1	2.15	4-24-15	58.7	1.13
			4-22-15	49.4	2.19			
			4-24-2	51.0	2.25			
			4-24-17	53.0	2.29			

Meniscus Length L in Cm. Vs P_0/P_1

TABLE III

		Run No.	P_o/P_1	P_o	$\dot{m}_f$	$\dot{m}_f$		Meniscus Length
				PSIA	Slugs/sec	Slugs/sec		C_M
					$\times 10^{-6}$	$\times 10^{4}$		Measured
		4-22-6	28.3	54.9		31.0		1.70
		4-22-4	29.9	56.9		32.1		1.70
$\alpha = 0°$		4-22-3		64.0		36.1		
Straight		4-22-8	40.2	78.0		44.0		1.90
Nozzle		4-22-7		90.8		51.2		
		4-22-2	48.6	94.5		53.4		2.15
		4-21-3	50.5	97.8		55.1		2.10
		4-24-4	28.95	55.8		31.5		1.46
		4-24-6	31.7	60.9		34.3		1.70
$\alpha = 14°$		4-22-13	44.6	85.9		48.4		2.06
		4-22-14	45.1	86.9		49.0		1.98
Straight		4-22-16	48.1	92.9		52.2		2.15
Nozzle		4-22-15	49.4	95.9		54.0		2.19
		4-24-2	51.0	97.8		55.0		2.25
		4-24-3		99.6		56.1		
		4-24-7	53.0	101.3		58.0		2.29
		4-24-13		52.8		6.7		
		4-24-14	31.1	59.9		7.6		.70
$\alpha = 14°$		4-24-11	44.0	84.9		10.39		.91
		4-24-12	45.8	87.9		10.59		.96
Divergent		4-24-8		104.3		13.28		
Nozzle		4-24-9	57.5	104.9		13.33		1.09
		4-24-15	58.7	106.5		13.52		1.13
		Variation of Meniscus Length (ℓ)						
		with P_o/P_1 and with $\dot{m}_f$						
		Table IV						

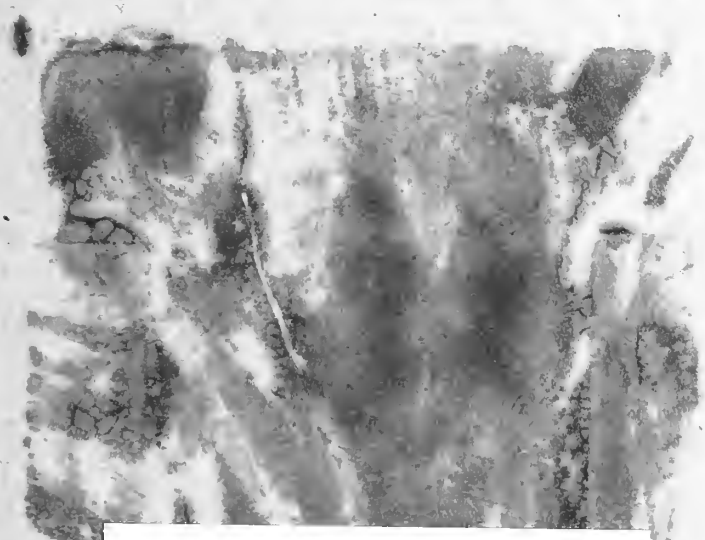

Thesis 12987
P53 Pierce
An investigation of the effects of a side control jet on the normal force, drag, and moment of an airborne body in supersonic flight.

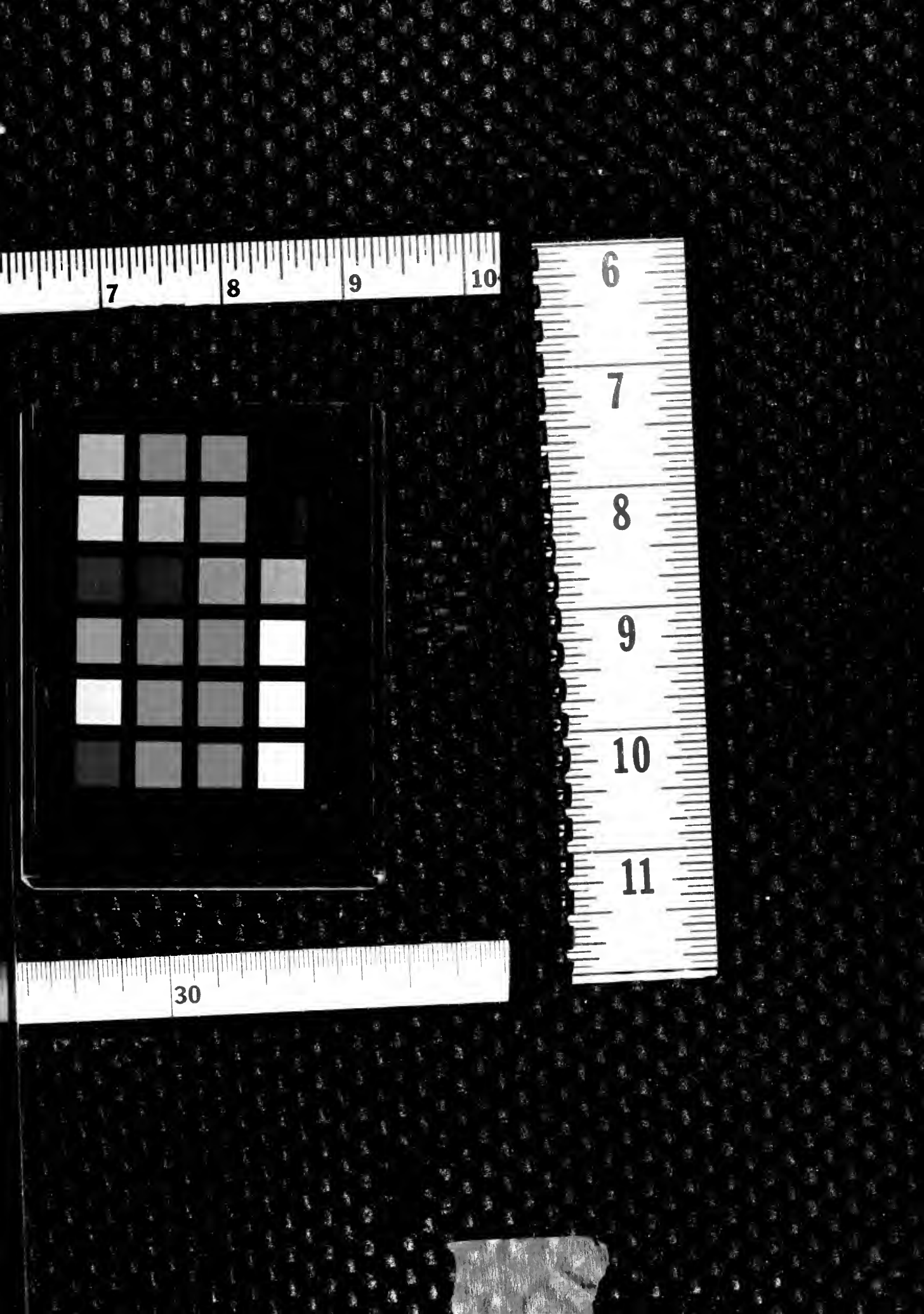
7
8
9
10
6
7
8
9
10
11
30